Article

Cell Metabolism

Human Tolerogenic Dendritic Cells Regulate Immune Responses through Lactate Synthesis

Graphical Abstract

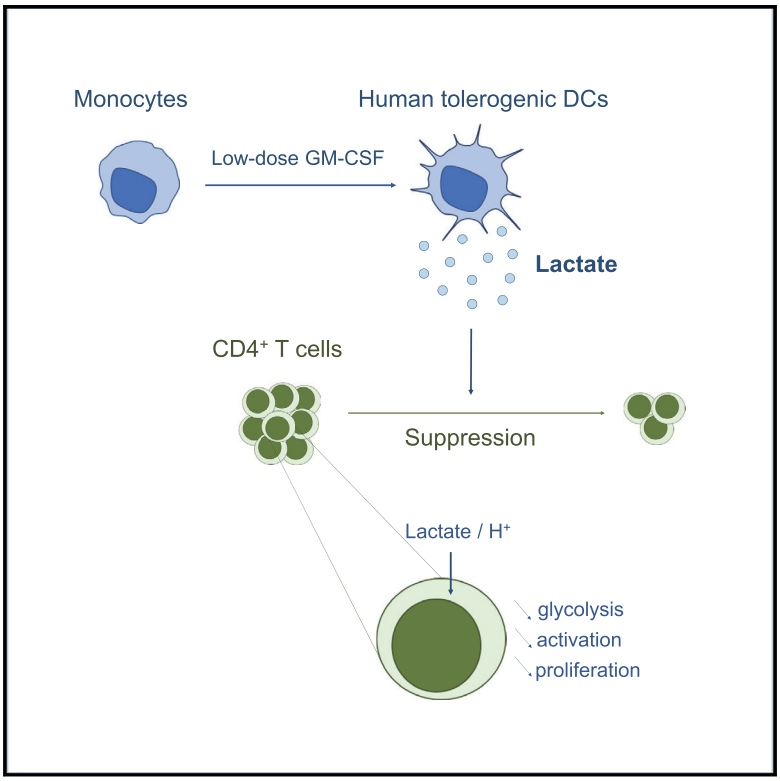

Authors

Eros Marin, Laurence Bouchet-Delbos, Ophélie Renoult, ..., Claire Pecqueur, Maria-Cristina Cuturi, Aurélie Moreau

Correspondence

aurelie.moreau@univ-nantes.fr

In Brief

Human autologous tolerogenic dendritic cells (ATDCs) are currently being evaluated in a clinical trial as a cell-based immunotherapy for kidney transplant recipients. Marin et al. report that ATDCs are glycolytic and produce high amounts of lactate. This secreted lactate is taken up by T cells, reducing their glycolytic flux and shifting T cell responses toward tolerance, thereby delaying graft-versus-host disease.

Highlights

- Monocyte-derived human tolerogenic dendritic cells (TolDCs) are glycolytic
- TolDCs produce high amounts of lactate, which suppresses T cell proliferation
- TolDC-secreted lactate taken up by T cells reduces their glycolysis and differentiation
- TolDCs delay xeno-GVHD development and promote a transient increase of lactate

Marin et al., 2019, Cell Metabolism *30*, 1075–1090
December 3, 2019
https://doi.org/10.1016/j.cmet.2019.11.011

CellPress

Cell Metabolism
Article

Human Tolerogenic Dendritic Cells Regulate Immune Responses through Lactate Synthesis

Eros Marin,[1,12] Laurence Bouchet-Delbos,[1,12] Ophélie Renoult,[2] Cédric Louvet,[1] Véronique Nerriere-Daguin,[1,3] Amy J. Managh,[4] Amandine Even,[1] Matthieu Giraud,[1] Thien Phong Vu Manh,[5] Audrey Aguesse,[6] Gaelle Bériou,[1] Elise Chiffoleau,[1] Brigitte Alliot-Licht,[1,7] Xavier Prieur,[8] Mikael Croyal,[6] James A. Hutchinson,[9] Natasa Obermajer,[10] Edward K. Geissler,[9] Bernard Vanhove,[1,3] Gilles Blancho,[1] Marc Dalod,[5] Régis Josien,[1,11] Claire Pecqueur,[2,3] Maria-Cristina Cuturi,[1,3,13] and Aurélie Moreau[1,3,13,14,*]

[1]Centre de Recherche en Transplantation et Immunologie UMR1064, INSERM, Université de Nantes, CHU Nantes, ITUN, Nantes, France
[2]Centre de Recherche en Cancérologie et Immunologie Nantes-Angers UMR1232, INSERM, Université de Nantes, Nantes, France
[3]LabEx IGO "Immunotherapy, Graft, Oncology", Nantes, France
[4]Centre for Analytical Science, Department of Chemistry, Loughborough University, Loughborough, UK
[5]Centre d'Immunologie de Marseille-Luminy, Aix-Marseille Université, CNRS, INSERM, CIML, Marseille, France
[6]UMR 1280 PhAN, Mass Spectrometry Core Facility, INRA, CRNHO, West Human Nutrition Research Center, Nantes, France
[7]Faculté d'Odontologie, Université de Nantes, Nantes, France
[8]Institut du Thorax, INSERM, CNRS, Université de Nantes, Nantes, France
[9]Department of Surgery, University Hospital Regensburg, Regensburg, Germany
[10]Division of Surgical Oncology, University of Pittsburgh, Hillman Cancer Center, Pittsburgh, PA, USA
[11]Laboratoire d'Immunologie, CHU Nantes, Nantes Université, Nantes, France
[12]These authors contributed equally
[13]These authors contributed equally
[14]Lead Contact
*Correspondence: aurelie.moreau@univ-nantes.fr
https://doi.org/10.1016/j.cmet.2019.11.011

SUMMARY

Cell therapy is a promising strategy for treating patients suffering from autoimmune or inflammatory diseases or receiving a transplant. Based on our preclinical studies, we have generated human autologous tolerogenic dendritic cells (ATDCs), which are being tested in a first-in-man clinical trial in kidney transplant recipients. Here, we report that ATDCs represent a unique subset of monocyte-derived cells based on phenotypic, transcriptomic, and metabolic analyses. ATDCs are characterized by their suppression of T cell proliferation and their expansion of Tregs through secreted factors. ATDCs produce high levels of lactate that shape T cell responses toward tolerance. Indeed, T cells take up ATDC-secreted lactate, leading to a decrease of their glycolysis. *In vivo*, ATDCs promote elevated levels of circulating lactate and delay graft-versus-host disease by reducing T cell proliferative capacity. The suppression of T cell immunity through lactate production by ATDCs is a novel mechanism that distinguishes ATDCs from other cell-based immunotherapies.

INTRODUCTION

Current therapies for autoimmune diseases and allograft rejection generally involve the continuous use of non-specific immunosuppressive drugs that are associated with increased risks of infections, certain types of cancer, and toxicities. Cell-based immunotherapy with *ex vivo*-generated tolerogenic dendritic cells (DCs) has long been recognized as an efficient means of promoting antigen-specific tolerance. As previously reported by our group and others, administration of these tolerogenic DCs to rodents prevents various autoimmune diseases (Machen et al., 2004; Mansilla et al., 2015; Stoop et al., 2011) and rejection of allografts (Baas et al., 2014; Hill et al., 2011; Lutz et al., 2000; Segovia et al., 2014; Turnquist et al., 2007). The potency of tolerogenic DC therapy in the induction of tolerance was linked to

Context and Significance

Cell therapy is a promising strategy for treating patients suffering from autoimmune or inflammatory diseases or receiving a transplant. The first clinical trials using tolerogenic dendritic cells (tolDCs) are in progress; therefore, a more complete understanding of their mechanisms of action is required. Researchers at Nantes University and INSERM have found that a class of *in vitro*-generated tolDCs used in the clinic produces a high amount of the metabolite lactate, which effectively reduces glycolytic metabolism of T cells. This metabolic impairment effectively suppresses the immune response by inhibiting T cell proliferation and differentiation to effector cells. Lactate-secreting cells, such as the dendritic cells used in this study, may be considered as an interesting therapeutic approach toward immunosuppressive therapy.

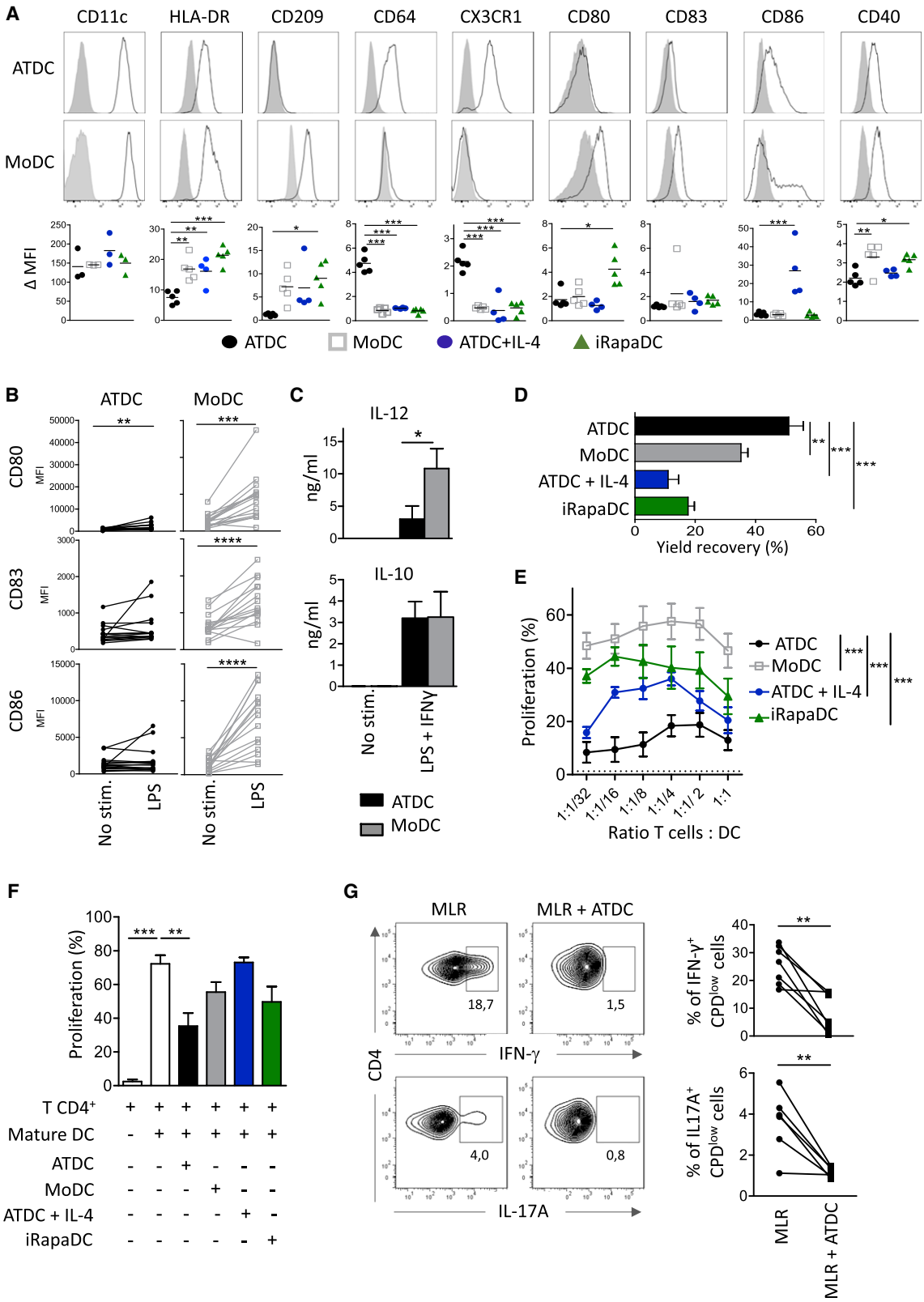

Figure 1. Human ATDCs Display Tolerogenic Features

(A) Expression of markers by ATDCs and MoDCs (black line) and their respective isotype controls (gray shaded) (representative of n ≥ 4 donors; Figure S1). Scatterplots depict MFI marker/MFI isotype control ratios in generated DCs (n ≥ 3 donors).

(legend continued on next page)

an enrichment of Tregs and to the inhibition of T cell proliferation. Tolerogenic DCs act on T cells with contact-dependent mechanisms mediated by molecules such as PD-L1, Fas-L, or immunoglobulin-like transcripts (ILTs) and with contact-independent mechanisms mediated by cytokines such as interleukin (IL)-10 and TGF-β or by immunomodulatory molecules such as indoleamine-2,3-dioxygenase (IDO) and inducible nitric oxide synthase (iNOS) (Marín et al., 2018).

In humans, tolerogenic DCs have been generated by exposure of blood monocytes to growth factors, cytokines, or pharmacological agents (Marín et al., 2018). Our previous studies in mice and non-human primates demonstrated the robustness of a low-dose GM-CSF (granulocyte-macrophage-colony stimulating factor) protocol (in the absence of other cytokines or agents) to generate so-called autologous tolerogenic DCs (ATDCs) (Moreau et al., 2009; Segovia et al., 2014). We also validated the safe administration of these cells in non-human primates (Moreau et al., 2014). Strategies for the preparation of clinical-grade monocyte-derived tolerogenic DCs have emerged only within the last few years and have enabled groups to investigate the therapeutic potential of these DCs in patients suffering from autoimmune or inflammatory diseases (Kim et al., 2018). Based on our expertise, we developed a GMP-compatible process for producing human ATDCs. These cells are currently being administered to kidney transplant recipients in a first-in-man phase I/II clinical trial to evaluate the safety and efficacy of this cellular immunotherapy in solid organ transplantation (NTC0225055).

Here, we characterize human ATDCs on the basis of analysis of their phenotype and transcriptome, their suppressive properties, and their glycolytic metabolism. Interestingly, ATDCs create a lactate-rich environment conducive to immunosuppression. This environment dysregulates the aerobic glycolysis of T cells and suppresses their proliferation, as well as induces the expansion of regulatory T cells (Tregs). The relationship between lactate production and the therapeutic activity of human ATDCs was then investigated in a human-into-mouse graft-versus-host disease (GVHD) model. The mechanistic insights gained from this research are immediately relevant to the interpretation of our clinical trial and provide a further rationale for extending the clinical applications of ATDC therapy to other clinical indications.

RESULTS

Human ATDCs Are T Cell-Suppressive DCs

ATDCs were obtained after a 6-day culture of monocytes in serum-free AIMV medium (clinical grade medium) supplemented with 100 IU/mL of GM-CSF. For a comparator population in all subsequent experiments, we used classic monocyte-derived DCs (MoDCs) that were obtained by culturing monocytes in RPMI-FCS medium supplemented with GM-CSF and IL-4 for 6 days. Because protocols for the generation of ATDCs and MoDCs differ by both the medium and the addition of IL-4, we also analyzed the impact of IL-4 on ATDCs (ATDCs + IL-4). Lastly, ATDCs were compared to another population of reported tolerogenic DCs (Macedo et al., 2013; Monti et al., 2003; Woltman et al., 2001) generated in presence of GM-CSF, IL-4, and rapamycin (iRapa-DCs).

An extensive phenotyping of ATDCs and MoDCs (Figures 1A and S1) revealed that ATDCs shared a common expression profile associated with naturally occurring myeloid DC subsets (Cao et al., 2006; Goudot et al., 2017; Haniffa et al., 2015; Merad et al., 2013; See et al., 2017; Segura et al., 2013) (Table S1), namely $CD11c^+$, $HLA\text{-}DR^+$, $CD1c^+$, and $CD141^+$. Both ATDCs and MoDCs expressed CD11b, CD206, CCR2, and CCR7. Critically, in contrast to MoDCs and other populations tested (ATDC + IL-4 and iRapa-DCs), ATDCs did not express CD209 (DC-SIGN) but expressed markers usually associated with monocyte-derived macrophages, such as CD64 and CX_3CR1. ATDCs were further characterized as $CD1a^-$, $Fc\varepsilon R1^-$, $CD123^+$, $CCR5^+$, $CCR9^{low}$, $PD\text{-}L1^-$, $HLA\text{-}G^-$, $ILT\text{-}2^+$, $ILT\text{-}3^+$, $ILT\text{-}4^-$, and $ILT\text{-}7^-$ cells (Figure S1). Taking together and considering our previous animal studies, we regard human ATDCs as dendritic cells with certain macrophage-like features.

In agreement with a tolerogenic profile, ATDCs displayed an immature phenotype ($HLA\text{-}DR^{low}CD80^{-/low}CD86^{low}CD83^-CD40^{low}$), whereas other generated DCs (MoDCs, ATDCs + IL-4, and iRapa-DCs) express higher levels of these markers (Figures 1A and S1B). Furthermore, ATDCs maintain their immature state (with no overexpression of CD83 and CD86 and a weak increase of CD80 expression) after exposure to LPS (Figures 1B and S2A) or other TLR ligands (Figure S2B). In contrast, MoDCs strongly upregulated co-stimulatory molecules under the same experimental conditions (Figure 1B). Strikingly, even after a strong stimulation with LPS and interferon-γ (IFNγ), ATDCs secreted IL-10 but produced significantly less IL-12 than MoDCs did (Figure 1C). Furthermore, TLR5 and TLR7-8 stimulations favored IL-10 secretion by ATDCs in the absence of IL-12 production (Figure S2B). ATDCs also expressed CCR7 (Figure S1A), implying an ability to migrate into secondary lymphoid organs. TLR ligation increased CCR7 expression on ATDCs (Figure S2B), suggesting that *in vivo*, the triggering of TLRs on ATDCs would favor their migration to secondary lymphoid organs while maintaining their tolerogenic potential. A better yield was observed in ATDCs as compared with other DCs (Figure 1D), which is an important point for their use in clinical trial. Rapamycin was previously reported to induce apoptosis of MoDCs (Monti et al., 2003; Woltman et al., 2001).

Tolerogenic DCs are also defined by their ability to control T cell proliferation. ATDCs were poor stimulators of allogeneic T cell proliferation in mixed lymphocyte reaction (MLR)

(B) ATDCs and MoDCs were either treated or not treated with LPS ($n \geq 14$ donors).
(C) IL-10 and IL-12p70 concentrations in supernatants of DCs either stimulated or not stimulated with LPS-IFNγ ($n \geq 4$ donors).
(D) Percentage of cell recovery ($n \geq 4$ donors).
(E) DCs were cultured with allogeneic CPD-labeled $CD3^+$ T cells at different T:DC ratios. T cell proliferation was assessed by CPD dilution ($n \geq 3$ donors).
(F and G) CPD-labeled $CD4^+$ T cells were cultured with allogeneic mature DCs in the presence or absence of DCs (autologous to T cells).
(F) T cell proliferation (as described in E) ($n \geq 3$ donors).
(G) Plots depict the percentage of $CD4^+IFN\gamma^+$ and $CD4^+IL\text{-}17^+$ cells; graphs show cumulative data of $n \geq 6$ donors.
p values were calculated by one-way ANOVA in (A), (D), and (F); by paired t tests in (B), (C), and (G); and by two-way ANOVA in (E). $^*p < 0.05$, $^{**}p < 0.01$, $^{***}p < 0.001$.

A

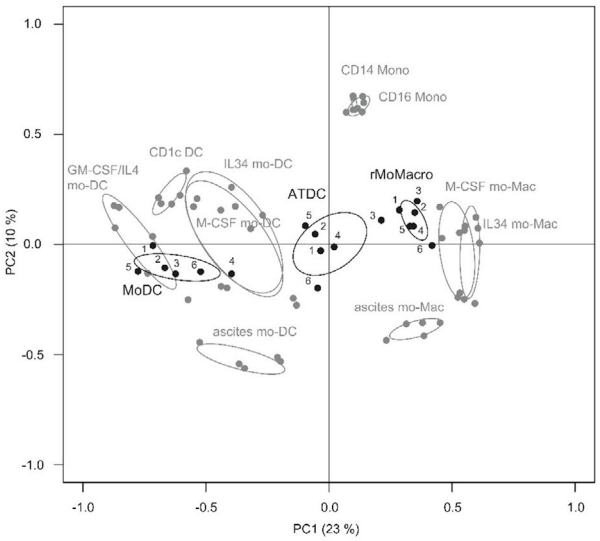

B

Biological processes reduced in ATDCs/MoDCs

Gene sets	NES	p-value
TGF-β signaling	-1,45	0,0282
Allograft rejection	-1,40	0,0052
WNT-β catenin signaling	-1,39	0,0664
TNF-α signaling via NFκB	-1,35	0,0101
Estrogen early response	-1,27	0,0439
Inflammatory response	-1,25	0,0455

Biological processes enriched in ATDCs/MoDCs

Gene sets	NES	p-value
G2/M checkpoint	2,20	0,0000
E2F targets	2,20	0,0000
Mitotic spindle	1,54	0,0003
Myc targets v2	1,32	0,0768
Mtorc1 signaling	1,32	0,0253
Glycolysis	1,28	0,0425

C

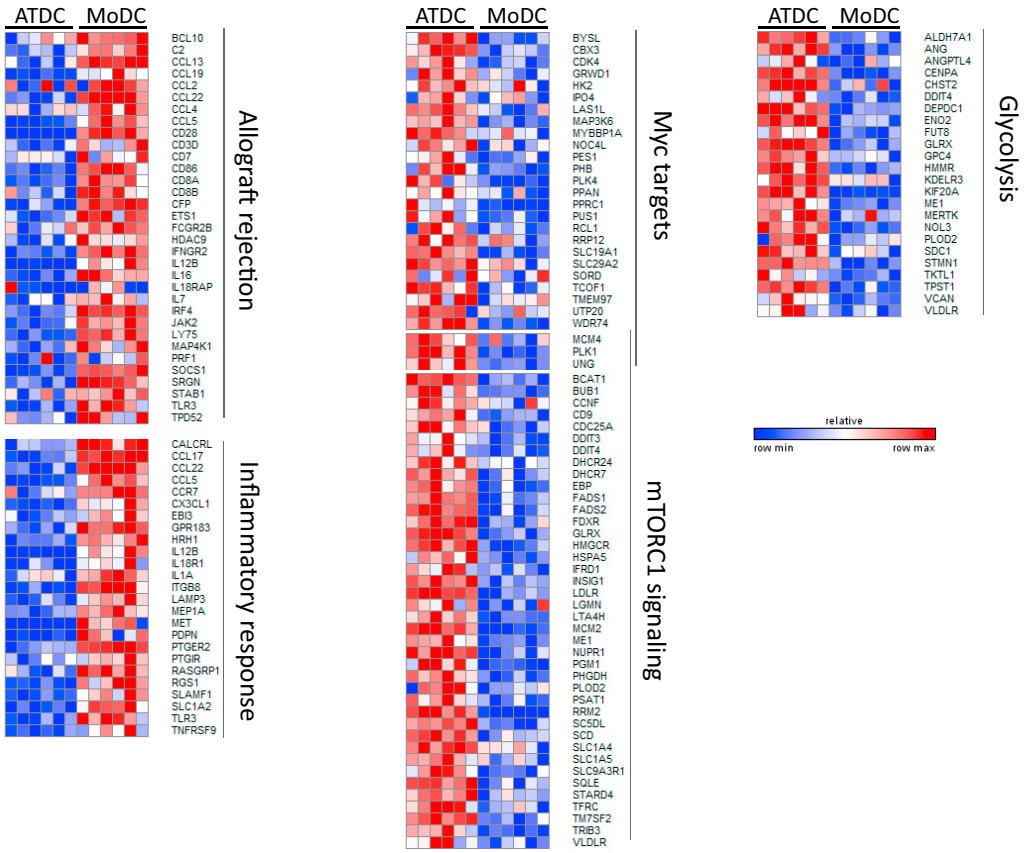

Figure 2. Comparison of ATDCs with Monocytes and *In Vitro*- and *In Vivo*-Derived Cells

(A) Microarrays were performed on ATDCs, MoDCs, and rMoMacros generated from monocytes of 6 donors. Transcriptomic data of these populations (black) were compared with human populations obtained from public datasets (Goudot et al., 2017) (gray). This graph depicts the principal component analysis of these different subsets. Numbers indicate the donor ID used to generate ATDCs, MoDCs, and rMoMacros.

(legend continued on next page)

(Figure 1E) and were able to significantly suppress $CD4^+$ T cell proliferation induced by mature DCs (Figure 1F). This suppression was associated with an inhibition of IFNγ- and IL-17-producing T cells (Figure 1G). In comparison, immature MoDCs and other DC populations stimulated allogeneic T cell proliferation more potently and were significantly less efficient than ATDCs in suppressing $CD4^+$ T cell proliferation (Figures 1E and 1F). Taken together, these results demonstrate the strong tolerogenic profile of ATDCs. ATDCs clearly display greater capacity than iRapa-DCs to suppress T cell responses *in vitro*. Furthermore, the absence of IL-4 during ATDC generation is a key component for promoting their suppressive potential.

ATDCs Exhibit a Unique Transcriptomic Profile

We next compared the profile of ATDCs to that of other monocyte-derived cells by transcriptomic analyses of paired ATDCs, MoDCs, and resting monocyte-derived macrophages (rMoMacros), all of which were produced from the same 6 donors. Expression data from our *in vitro*-generated ATDCs, MoDCs, and rMoMacros (in black) were compared with previously published expression datasets (in gray) (Goudot et al., 2017) from monocytes, *in vitro*-derived DCs and macrophages, and *in vivo* DCs and macrophages in a principal component (PC) analysis (Figure 2A). We validated the combined analysis of all these datasets by the observation that the cell types differentiated within the same protocol between the public data (GM-CSF/IL-4 MoDCs) and our study (MoDCs) clustered together. Furthermore, our rMoMacro clustered close to the *in-vitro*-differentiated M-CSF mo-Mac (monocyte-derived macrophage).

In our analysis, PC1 clearly separates DCs and macrophages, whereas PC2 distinguishes monocytes, *in vitro*-monocyte-differentiated cells, and *in vivo*-monocyte-differentiated cells from ascites. This analysis highlighted that ATDCs represent an individual subtype of cells that is distinct from monocytes, DCs, or macrophages (Figure 2A). Because ATDCs are refractory to TLR-mediated signals (Figures 1B, 1C, and S2), we consider ATDCs to be a unique, maturation-resistant population of monocyte-derived DCs. The uniqueness of ATDCs was also illustrated by the full list of genes with expression fold change over 2 in ATDCs versus MoDCs and rMoMacros (Table S2). We then computed the rank of gene expression in ATDCs versus MoDCs to assess the pathway enrichment in these samples with gene set enrichment analysis (GSEA). Interestingly, gene sets associated with allograft rejection and inflammatory response were reduced in ATDCs compared with MoDCs (Figures 2B and 2C), thus corroborating our findings that ATDCs have tolerogenic properties. Furthermore, the observation that ATDCs exhibited significant enrichments of genes associated with glycolysis, Myc targets, and mTORC1 signaling (Figures 2B and 2C) prompted us to investigate the glycolytic activity of ATDCs.

ATDCs Are Highly Glycolytic Cells

To study glycolysis in ATDCs, we first investigated their glucose consumption. ATDCs and MoDCs were cultured alone for 6 days in the same medium, and the culture supernatants (SNs) were analyzed (ATDC SN and MoDC SN). In accordance with our transcriptomic results, ATDCs strongly took up glucose from the media (Figure 3A). Once taken up by cells, glucose is converted to pyruvate, which is then converted to lactate or imported into the mitochondria to fuel the tricarboxylic acid (TCA) cycle. In order to determine whether ATDCs use the oxidative pathway or the aerobic glycolysis, we performed Seahorse analyses. ATDCs converted more glucose to lactate than did MoDCs, as shown by basal extracellular acidification rate (ECAR) (Figure 3B). To better characterize glucose fate in ATDCs and MoDCs, similar experiments were performed before and after glucose addition in the media. Although ATDCs and MoDCs in absence of glucose displayed similar ECAR levels, the addition of glucose strongly increased ECAR values in ATDCs but not in MoDCs (Figure 3C). In fact, glucose conversion to lactate represented around 50% of maximal glycolytic ability of MoDCs whereas ATDCs used up to 80% of their maximal ability. Regarding their oxidative capacity, ATDCs also displayed a higher basal oxygen consumption rate (OCR) than did MoDCs, as well as displaying higher ATP-linked respiration and maximal respiration (Figure 3D). Contribution of lipid to mitochondrial respiration was investigated by the addition of exogenous palmitate with or without etomoxir, an inhibitor of fatty acid entry in the mitochondria. Surprisingly, ATDCs did not use exogenous palmitate to fuel the TCA, whereas these exogenous lipids efficiently contributed to MoDC respiration (Figure 3E). However, ATDCs may use endogenous fatty acids as shown by the decrease of OCR value below its basal level after addition of etomoxir (Figure 3E). In agreement with these results, ATDCs displayed a significant amount of lipid droplets, but none could be detected in MoDCs (Figure 3F). Interestingly, the higher basal glycolysis and respiration observed in ATDCs were associated with an enhanced intracellular ATP concentration (Figure 3G). Besides glucose and lipids, other substrates such as amino acids can be oxidized. Mass spectrometry analysis performed on ATDC SN and MoDC SN revealed that ATDCs consumed higher amounts of amino acids than did MoDCs (Figure 3H), suggesting that amino acids might be an additional mitochondrial fuel efficiently used in ATDCs. ^{13}C glucose experiments confirmed that glucose taken up by ATDCs was more efficiently converted to lactate than glucose taken up by MoDCs, but glucose taken up by ATDCs also fueled the TCA (Figure 3I). A higher amount of lactate was observed in ATDCs whereas similar amounts of TCA metabolites were detected in ATDCs and MoDCs (Figure 3I). Furthermore, ATDCs overexpressed the lactate transporter, monocarboxylate transporter 1 (*MCT1*), and pyruvate dehydrogenase kinases (PDKs) 1 and 4 (Figure 3J). PDK enzymes inhibit pyruvate deshydrogenase (PDH), which allows the production of Acetyl-CoA from glycolytic pyruvate.

To further investigate aerobic conversion of glucose to lactate in ATDCs, we measured lactate dehydrogenase (LDH) activity and lactate secretion. ATDCs displayed higher LDH activity (Figure 3K) and produced more lactate than the other types of DCs we analyzed in Figure 1 and led to a pH acidification (Figure 3L). Taken together, these results showed that ATDCs are strong glycolytic cells and secrete high amounts of lactate.

(B and C) We performed GSEA on ATDC versus MoDC transcriptomic data with the lists of "hallmark gene sets" from the Molecular Signature Database. The tables show the gene sets reduced or enriched in ATDCs versus MoDCs (B), whereas heatmaps depict genes that contributed the most to pathway reduction or enrichment (C).

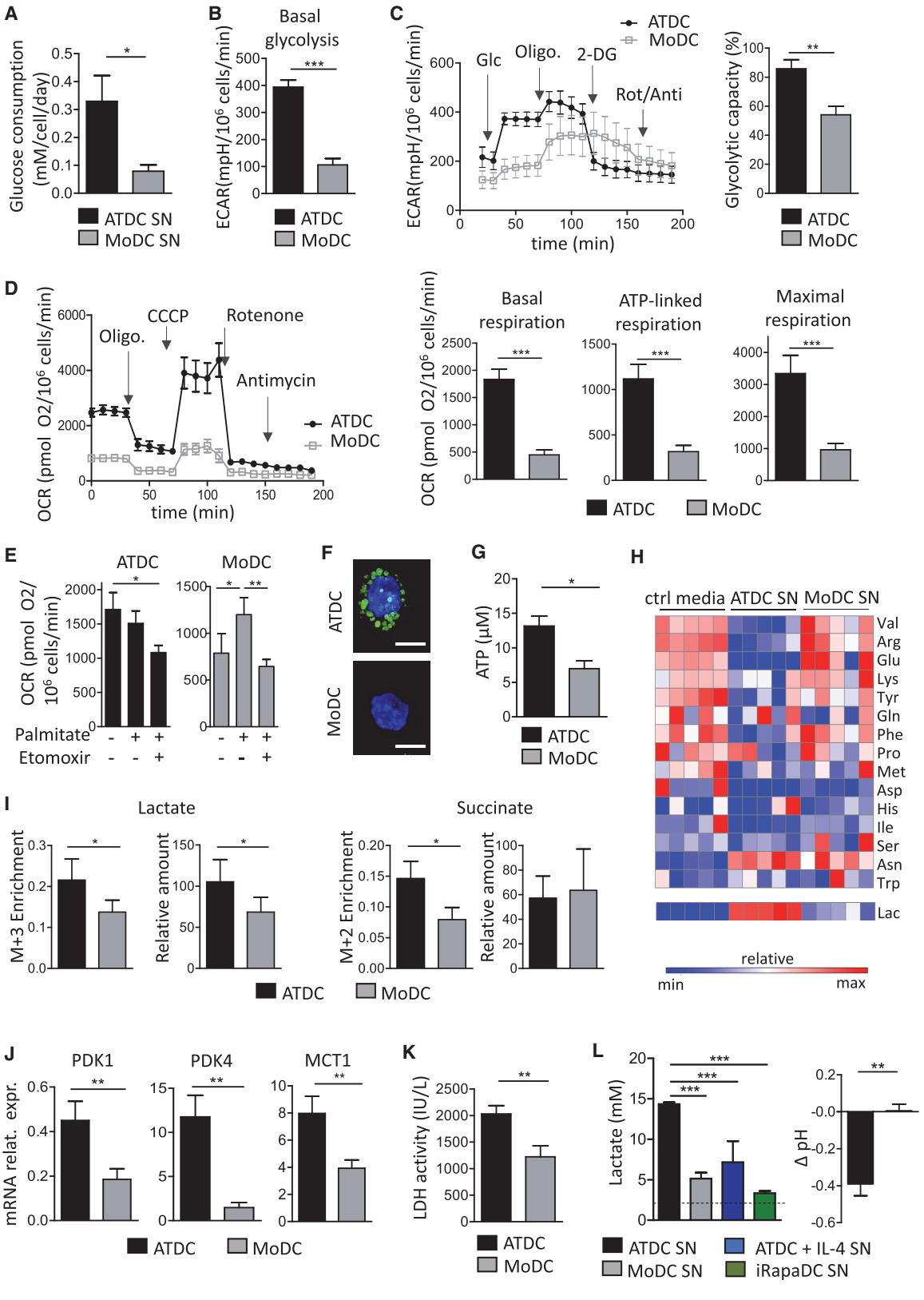

(legend on next page)

ATDCs Exert Their Immunomodulatory Function through a Non-classical Mechanism of Suppression

We next sought to clarify how ATDCs control $CD4^+$ T cell proliferation *in vitro* (as observed in Figure 1F). First, this suppression did not result from a competition between allogeneic stimulatory mature DCs and ATDCs because the addition of increasing numbers of stimulatory DCs did not impact suppression (Figure 4A). Second, to study their effects on ATDC-mediated suppression, we screened some known inhibitors of T cell proliferation produced by mononuclear phagocytes. TGF-β, IL-10, iNOS, and IDO were not involved in this suppression (Figures 4B and 4C). Furthermore, natural Tregs were not required for the suppressive activity of ATDC *in vitro* because the suppression of T cell proliferation was still observed with CD25-negative T cells (Figure 4D). Finally, neither induction of anergy nor apoptosis was responsible for ATDC-mediated suppression (Figures S3A and S3B).

We then asked whether ATDC-T cell interactions were required for the ATDC suppressive effect and performed experiments with transwell inserts. Surprisingly, ATDC suppression was mediated by a contact-independent mechanism because ATDCs reduced T cell proliferation independently of being present in the same compartment as T cells (Figure 4E). We corroborated this result by showing that the transfer of suppression assay medium (MLR + ATDC SN) was able to suppress a second MLR as efficiently as ATDCs were themselves, indicating that soluble factors produced, or induced, by ATDCs were involved in T cell suppression (Figure 4F). To determine whether these soluble factors were produced by ATDCs or by other cell types present in the assay (T cells and mature DCs), we transferred ATDC SN and MoDC SN into a new MLR. As shown in Figure 4G (white bars), the secretome of ATDCs was responsible for T cell suppression whereas MoDC SN did not modify T cell proliferation. Furthermore, only the fraction of ATDC SN containing molecules under 3 KDa (excluding most of the proteins) efficiently inhibited T cell proliferation (Figures 4G and S3C).

We then hypothesized that ATDCs might suppress T cell proliferation either by nutrient deprivation or by secretion of lactate. Measurement of glucose at the end of the culture confirmed that ATDCs strongly consumed glucose from the medium (Figure 4H). However, addition of glucose, glutamine, or pyruvate to the suppression assay did not abrogate ATDC's suppressive ability, demonstrating that nutrient deprivation was not responsible for the ATDC suppressive effect (Figures 4I, S3D, and S3E). Strikingly, we found a high amount of lactate (around 10 mM) in the suppression-assay condition (Figure 4J). Therefore, we hypothesized that lactate secretion could be responsible for ATDC-mediated suppression rather than glucose deprivation.

Lactate Secreted by ATDCs Is Involved in Their Suppressive Activity

It has been reported that tumor-derived lactate impairs T cell proliferation and effector functions (Brand et al., 2016; Fischer et al., 2007). Based on these works, we investigated the role of ATDC-derived lactate *in vitro*. Induction of ATDC and MoDC apoptosis at effective concentrations of oxamic acid and GSK2837808A precluded the use of these two inhibitors of LDH activity (data not shown). Nevertheless, Fischer et al. demonstrated that the neutralization of lactate with NaOH abrogated its suppressive effect (Fischer et al., 2007). We first confirmed in an MLR context that lactate alone, as well as acidification alone, did not significantly impair $CD4^+$ T cell proliferation (Figure 5A). However, a decrease of proliferation was observed when T cells were cultured with 10 mM of lactate (amount of lactate detected in the suppression assay) plus 5 mM HCl (decrease of pH of 0.4 units) (Figure 5B), demonstrating that both acidification and lactate were required to inhibit T cell proliferation. To test the involvement of lactate secreted by ATDCs, we then neutralized ATDC SN with 5 mM NaOH (increase of pH of 0.46 units) before its addition to the suppression assay (Figure 5C). Our results showed that neutralization of ATDC SN partially reversed T cell suppression (Figure 5D) and suggested that ATDC-derived lactate inhibits $CD4^+$ T cell proliferation. Furthermore, ATDC SN induced a decrease of CCND1, IFNγ, and tumor necrosis factor alpha (TNF-α) expressions in $CD4^+$ T cells, and this effect was partially abrogated in neutralizing conditions (Figures 5E–5G and S4A). These results are in accordance with our functional assays in which ATDCs suppressed T cell proliferation and inhibited Th1 differentiation (Figures 1F and 1G).

Tolerogenic DCs are known to induce both *de novo* generation and expansion of different types of regulatory T cells (Marín et al., 2018). Furthermore, Angelin et al. reported that a low glucose, high lactate environment favors the induction of Tregs at the

Figure 3. ATDCs Are Highly Glycolytic Cells

(A) ATDCs or MoDCs were cultured alone in RPMI-FCS medium. Glucose consumption was measured in SN at day 6 (n = 5 donors).

(B–E) Analysis of extracellular acidification rate (ECAR) (B and C) or oxygen consumption rate (OCR) (D and E). Initial medium was supplemented with glucose (B, D, and E) or not supplemented (C).

(B) Basal ECAR (n = 5 donors).

(C and D) ECAR and OCR were measured after sequential stimulations with the molecules mentioned in respective graphs (n = 5 donors).

(E) OCR were measured in DCs either cultured or not cultured with palmitate in absence or presence of etomoxir (n = 6 donors).

(F) Lipid uptake (green) were observed following incubation with lipids (one experiment representative of 3). Scale bar, 5 μm.

(G) Intracellular ATP was measured after differentiation (n = 4 donors).

(H) Metabolomic analysis was performed on SN from DCs of 5 donors. Media without cells of each experiment were used as controls. Heatmap illustrates the relative levels of several metabolites.

(I) ATDCs and MoDCs were incubated with ^{13}C glucose. Enrichments of lactate and succinate, as well as relative amount of these metabolites, were measured (n = 10 donors).

(J) Relative expression of indicated molecules in DCs (n ≥ 6 donors).

(K) Lactate dehydrogenase (LDH) activity quantified in cells (n = 6 donors).

(L) Lactate concentration was measured in different DC SN (n = 6 donors, except ATDC + IL-4, n = 3). Dotted line represents the amount measured in medium without cells. Δ pH was measured as pH of DC SN minus pH of RPMI (n ≥ 4 donors).

p values were calculated by paired t tests in (A)–(D), (G), and (I)–(K) and one-way ANOVA in (E) and (L); *p < 0.05, **p < 0.01, ***p < 0.001.

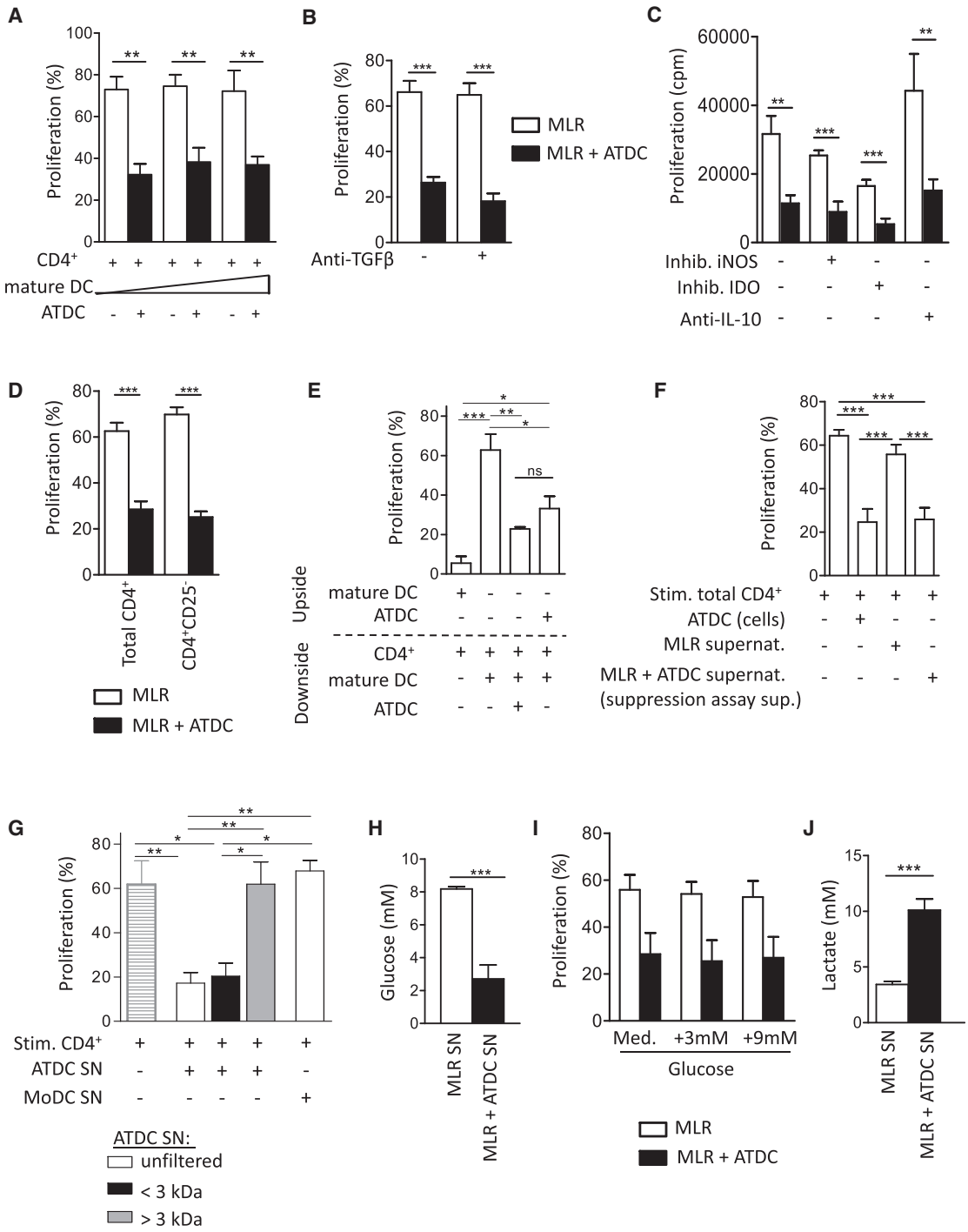

Figure 4. ATDCs Inhibit T Cell Proliferation by Soluble Factors

(A–G and I) ATDCs or ATDC SNs were added into MLR in different experimental conditions to understand how ATDCs inhibit $CD4^+$ T cell proliferation. In (A), (B), (D)–(G), and (I), proliferation was assessed by CPD dilution, whereas thymidine uptake was used in (C).

(A) $CD4^+$ T cells were cultured with different amounts of allogeneic mature DCs (5×10^4, 1×10^5, and 2×10^5) with or without autologous ATDCs (n = 3 donors).

(B and C) Anti-TGFβ, anti-IL-10, and inhibitors of IDO and iNOS were added in a suppressive assay (B, n = 6 donors; C, n ≥ 3 donors).

(D) Total $CD4^+$ T cells or $CD4^+CD25^-$ T cells were cultured with allogeneic mature DCs in the presence or absence of ATDCs (n = 12 donors).

(E) $CD4^+$ T cells were cultured with allogeneic mature DCs with or without ATDCs in a transwell assay (n = 3 donors).

(F) SNs from MLR or suppression assay (MLR + ATDC) were transferred to a new MLR (n ≥ 9 donors).

(G) DC SNs were transferred to a new MLR. ATDC SNs were filtrated on 3 KDa filter, and both fractions were tested and compared with unfiltrated SN conditions (n ≥ 3 donors; see also Figure S3C).

(legend continued on next page)

expense of effector T cells (Angelin et al., 2017). Our results showed that ATDC SN induced a higher percentage of $CD4^+$ $CD25^+FoxP3^{hi}$ Tregs among total $CD4^+$ T cells (Figures 5H and S4B) and an increase of *FOXP3* expression (Figure 5I). However, neutralization of ATDC SN did not abrogate its effects, suggesting that another soluble factor from ATDC secretome contributed to this Treg induction or that lactate secreted by ATDCs did not require acid environment to expand and/or generate Tregs. Because the percentage of Treg and Foxp3 expression increased in T cells cultured with ATDC SN, we investigated the effect of ATDC SN on expansion of $CD4^+CD25^+CD127^{low}$ natural Tregs *in vitro*. ATDC SN increased the expansion of these Tregs (Figure 5J). Furthermore, ATDC SN-expanded Tregs preserved their Foxp3 expression (Figure 5K) and their suppressive ability (Figure 5L). Taken together, these results showed that the secretome of ATDCs favors Treg expansion and inhibits total $CD4^+$ T cell proliferation and Th1 differentiation.

ATDC-Secreted Lactate Enters T Cells and Impairs Their Glycolytic Metabolism

Lactate can be taken up by cells through a MCT1 transporter that cotransports lactate and protons. Expression of *MCT1* was detected on $CD4^+$ T cells and upregulated after stimulation (Figure S4C). Fischer et al. previously demonstrated that lactate required acid environment to be transported by MCTs (Fischer et al., 2007). In this context, we confirmed that NaOH was able to block the uptake of lactate in T cells by using labeled lactate (Figure S4D). We then examined the capacity of $CD4^+$ T cells to take up ATDC-derived lactate. In the absence of stimulation, intracellular lactate was increased in $CD4^+$ T cells incubated with ATDC SN but not in $CD4^+$ T cells after incubation with ATDC SN neutralized with NaOH (Figure 6A). Similarly, increased lactate uptake was also observed in stimulated T cells with ATDC SN but was only partially reduced when ATDC SN was neutralized (Figure 6B). This partial reduction could possibly explain why neutralized ATDC SN only partially raised ATDC-mediated T cell suppression or IFNγ expression (Figures 5D and 5F). Furthermore, ATDC SN reduced glucose uptake (2-NBDG), *GLUT1* expression (glucose transporter), and *MYC* expression (transcription factor responsible for glycolysis induction) in stimulated T cells (Figures 6C–6E). These results suggest that increased intracellular lactate detected in T cells was because of increased lactate uptake rather than higher glycolytic activity. Because these metabolic changes are associated with decreased proliferation, these results further suggest that T cells are using lactate rather than glucose to fulfill their metabolic needs. The preferential use of lactate over glucose to fuel the TCA cycle has been previously shown in human non-small-cell lung cancer cells sustaining tumor metabolism (Faubert et al., 2017). To formally prove that a high amount of lactate (10 mM, as detected in suppression assay) can be taken up by T cells and process to the TCA, experiments with ^{13}C-lactate and ^{13}C-glucose were performed. As shown in Figure 6F, labeled lactate was taken up by T cells and processed in the TCA in a dose-dependent manner. Furthermore, a decrease of lactate and TCA metabolites derived from labeled glucose was observed in the presence of 10 mM lactate, demonstrating that high doses of lactate downregulate glycolysis (and possibly glucose uptake) (Figure 6F). Taken together, these results strongly suggest that ATDC-secreted lactate is taken up by T cells to fuel their TCA cycle and downregulates T cell glycolysis.

ATDCs Delay GVHD Development in Humanized Mice and Dampen T Cell Proliferation *In Vivo*

Injection of human PBMCs (peripheral blood mononuclear cells) into NSG (NOD-SCID-IL2rg$^{-/-}$) immunodeficient mice provides a reliable model of human-into-mice xenogeneic GVHD (Shultz et al., 2007). Prior to the clinical trial, we investigated ATDC fate after injection and whether ATDCs achieve regulatory activity *in vivo*. To this aim, irradiated NSG mice received human PBMCs in the presence or absence of autologous ATDCs (with the aim to mirror the clinical settings). As shown in Figures 7A and S5A, ATDC injection led to a significant delay in GVHD development that is shown by an increase in survival time and a reduction of weight loss in mice treated with ATDCs + PBMCs compared with mice treated with PBMCs alone. We then studied the fate of ATDCs after injection with gold nanoparticles-labeled ATDCs revealed by inductively coupled plasma mass spectrometry (ICP-MS). This highly sensitive technique allows the detection of rare cells in tissues (Managh et al., 2014) and did not modify the tolerogenic properties of ATDCs *in vitro* (Figures S5B–S5D). Gold-labeled ATDCs were tracked from day 3 to day 14 post cell injection, and the highest concentrations of ATDCs per mg of tissue were detected in liver, lung, and spleen; there was a peak at day 6 in the spleen (Figure 7B). Due to the respective weights of these organs, the total amount of Au was much higher in liver than in lung and spleen (Figure S6A). The accumulation of human myeloid cells after IV injection in these tissues has already been shown by others in humans (Hutchinson et al., 2011). In contrast, no gold staining was observed in heart and intestine, and low staining was present in kidney (data not shown). As gold was detected in homogenized tissue, it cannot be excluded that the detected signal was expressed by dead ATDCs or mouse phagocytic cells. A second technique was used to formally prove that gold staining coincided with the presence of viable ATDCs in the spleen where the adaptive immune response takes place. ATDCs were stained with Qtracker marker (Rosen et al., 2007), and splenocytes were analyzed by flow cytometry (Figures 7C and S6B). ATDCs, which represent less than 2% of total human $CD45^+$ cells, were still alive *in vivo* 6 days post-injection (viability reached 93.7% ± 5.1%; n = 5 mice). Furthermore, ATDCs maintained their immature phenotype and their negative expression of CD209 after injection, suggesting that ATDCs did not become immunogenic cells after injection (Figure 7C). Indeed, one of the major concerns associated with injection of tolerogenic DCs in humans is the risk that these cells become immunogenic DCs in response to inflammatory signals encountered *in vivo*. Strikingly, ATDCs

(I) MLR and suppression assays were performed with increasing concentrations of glucose. Glucose concentration of the RPMI medium is 9 mM (n = 3 donors). (H and J) Glucose (H) and lactate (J) concentrations were measured in the SN from MLR and MLR + ATDC conditions ($n \geq 9$ donors).

p values were calculated by two-way ANOVA in (A), (B), and (D) and by one-way ANOVA in (E)–(G), and paired t tests were used in (C), (H), and (J); $^*p < 0.05$, $^{**}p < 0.01$, $^{***}p < 0.001$.

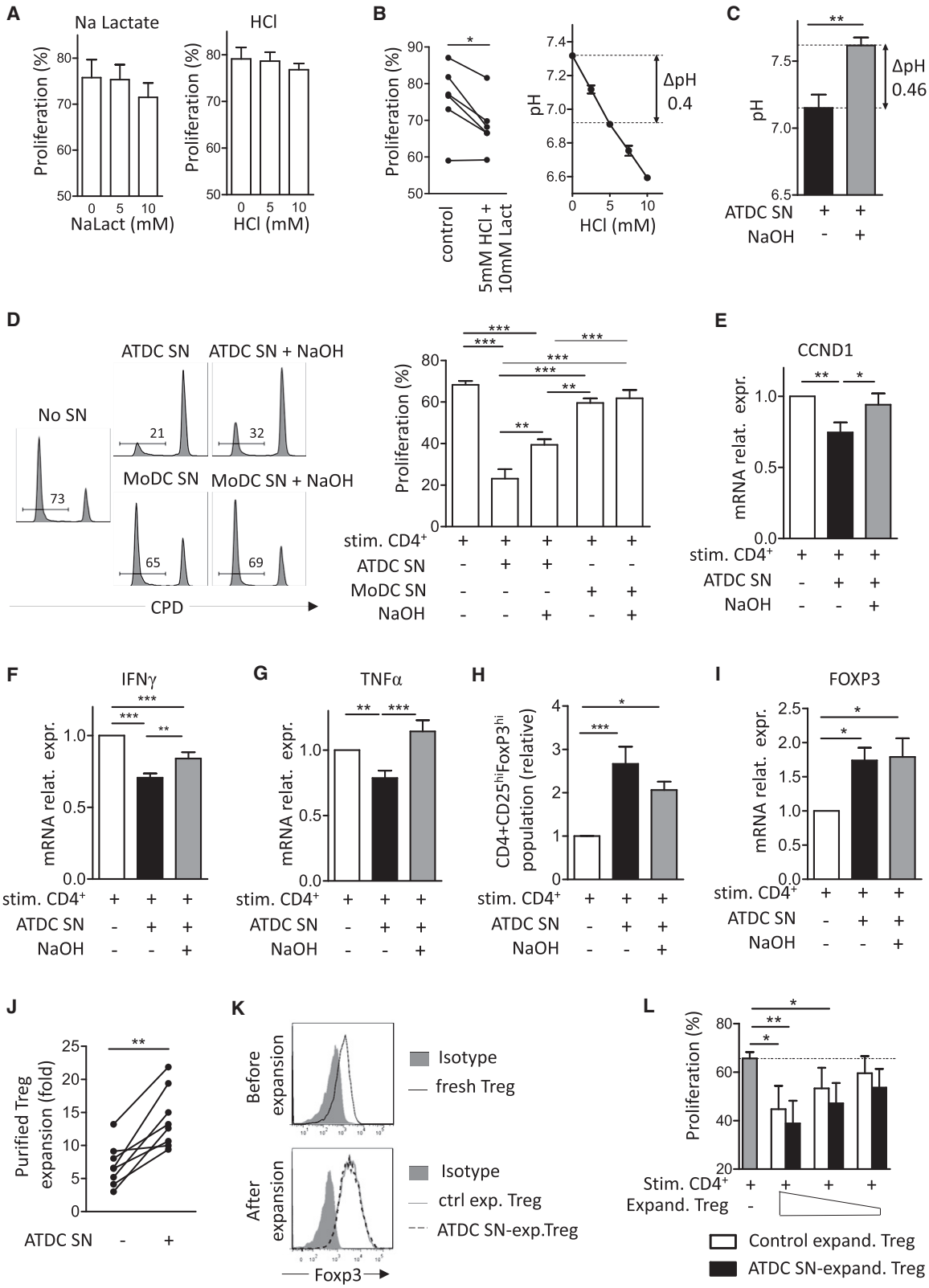

Figure 5. ATDC-Secreted Lactate Impairs CD4⁺ T Cell Proliferation

(A and B) MLRs were performed in the presence of increasing concentrations of Na lactate or HCl (A, n ≥ 3 donors) or in media containing 5mM HCl and 10mM lactate (B, n = 6 donors). T cell proliferation was assessed by CPD dilution. pH was quantified in medium with HCl at indicated doses at room temperature (n = 2 experiments).

(legend continued on next page)

also preserve the same expression of LDH after injection, suggesting that they kept a strong glycolytic capacity *in vivo*. Importantly, this result was supported by a transient increase of lactate concentration in the serum of mice receiving ATDCs one week after cell injection and detected with mass spectrometry (MS) (Figure 7D) and blood gas (Figure S6C) analyses.

Human cell reconstitution in blood and spleen did not appear modified between mice receiving or not receiving ATDCs over time (Figures S6D–S6F). Although some studies reported that Treg therapy prevented the development of xeno-GVHD in association with a reduction of human T cell engraftment (Cuende et al., 2015; Hippen et al., 2011; Mutis et al., 2006), others showed that Tregs, MDSCs, or a low dose of cyclosporine A delays GVHD development without reduction of cell engraftment (Chakraborty et al., 2013; Hannon et al., 2014; Søndergaard et al., 2013; Wang et al., 2019). In models of transplant arteriosclerosis and skin grafts in immunodeficient mice, injections of human Tregs also prevented graft rejections without reduction of human cell engraftments (Nadig et al., 2010; Zaitsu et al., 2017). This absence of correlation between treatment efficacy and the reduction of cell engraftment could be explained by the unspecific homeostatic proliferation that occurs in these immunodeficient mouse models and relies on non-classical mechanisms of cell activation (Tchao and Turka, 2012). In order to investigate the proliferative potential of T cells upon T cell receptor (TCR) ligation, we *ex vivo* stimulated splenocytes from both ATDC-treated and non-ATDC-treated mice with anti-CD3 and anti-CD28 antibodies. Our results highlighted that $CD4^+$ T cells from ATDC-treated mice displayed a lower proliferative capacity than those from control mice (Figure 7E) and suggested that ATDCs delay GVHD through the reduction of TCR-mediated proliferation of T cells. Taken together, our *in vivo* experiments showed that ATDCs delay GVHD development by controlling $CD4^+$ T cell proliferation in association with a transient increase of circulating lactate.

DISCUSSION

The role of lactate as an immunosuppressive metabolite has been well described in the tumor microenvironment (TME). Indeed, high lactate concentrations were detected in tumor biopsies, in correlation with metastatic spread and poor survival (Walenta et al., 2000). As early as 1927, Otto Warburg described that tumor cells rely on glycolysis even in the presence of oxygen (Warburg et al., 1927). This aerobic glycolysis is followed by increased lactate production by cancer cells, leading to an accumulation of lactate in the TME. A recent work showed that lactate, produced in cancer cells under tyrosine kinase inhibitors, could be an actor in tumor escape by instructing the TME to sustain an adaptive resistance to targeted therapies (Apicella et al., 2018). Furthermore, an elegant work from Zhang et al. showed that lactate was also a crucial compound of antiviral response escape because it negatively regulates RIG1-like receptors activation, leading to an inhibition of type 1 IFN induction (Zhang et al., 2019).

Back to the cancer field, previous works reported that lactate was able to suppress T cell proliferation and strongly diminish pro-inflammatory cytokine production in T cells (Brand et al., 2016; Fischer et al., 2007). Similarly, we showed that ATDCs create a lactate-rich environment that promotes lactate uptake by $CD4^+$ T cells and fuels TCA in these cells. On the basis of previous results, we could hypothesize that lactate accumulation impairs LDH kinetics in T cells and leads to a decrease in pyruvate to lactate formation and a decrease in NAD^+ refill, resulting in a decrease in GAPDH (glyceraldehyde 3-phosphate dehydrogenase) activity and a decrease in glycolytic activity (Angelin et al., 2017). Because glycolytic enzymes such as GAPDH favor inflammatory cytokine production (Chang et al., 2013), a reduced glycolytic activity could also explain the decreased expression of IFNγ and TNF-α in $CD4^+$ T cells cultured with ATDC SN. Our results also highlighted a reduced expression of cyclinD1 in T cells treated with ATDC SN, which was reversed in neutralized conditions. Interestingly, CyclinD1 expression is regulated by the metabolic sensor mTOR1 (Averous et al., 2008). Akt-mTOR signaling pathways have also been described to promote glycolysis (notably GLUT1 trafficking and *MYC* expression) and Th1/Th17 differentiation. It is thus highly possible that ATDCs control T cells by modulating these signaling pathways.

Inversely, the lactate-rich environment induced by ATDCs favored Treg expansion. These results are consistent with a study reporting that Tregs are not impaired by lactate and even preserve their immunosuppressive function through Foxp3 expression (Angelin et al., 2017). The authors showed that Foxp3 suppresses the *myc* gene and consequently downregulates glycolysis. Foxp3 also controls metabolic changes by the upregulation of oxidative phosphorylation (OXPHOS) and an increased NAD:NADH ratio that allow Treg functions under lactate-rich conditions (Angelin et al., 2017). However, our results showed that neutralization of ATDC SN does not affect the percentage of Tregs or the expression of Foxp3, suggesting that other soluble factors from ATDC SN are responsible for Treg induction. Another possible explanation is that lactate from ATDCs does not act on T cells and Tregs only through MCT

(C) pH was measured in ATDC SNs either neutralized or not neutralized with 5 mM NaOH and diluted with the same volume of RPMI medium (to mimic suppression assay) (n = 3 donors).
(D and H) SN from DCs, either neutralized or not neutralized with NaOH, were transferred to a new MLR.
(D) $CD4^+$ T cell proliferation was assessed by CPD dilution (one representative experiment and graph showing cumulative data of $\geq$8 donors).
(H) Proportions of $CD4^+CD25^+Foxp3^+$ cells (n = 12 donors).
(E–G and I) $CD4^+$ T cells were stimulated with PMA and ionomycin in the absence or presence of ATDC SN or NaOH-neutralized ATDC SN. Expressions of CCND1 (E, n = 16 donors), IFNγ (F, n = 18 donors), TNF-α (G, n = 17 donors), and Foxp3 (I, n = 12 donors). See also Figure S4A.
(J–L) Purified $CD4^+CD25^+CD127^{low}$ Tregs were expanded in presence or absence of ATDC SN.
(J) Fold of Treg expansion (n = 8 donors).
(K) Foxp3 expression (histograms representative of n = 5 donors).
(L) Suppressive ability (n = 8 donors) of Tregs.
p values were calculated by one-way ANOVA in (A) and (D)–(I); paired t tests in (B), (C), and (J); and unpaired t test was used in (L). No statistical difference was observed in (L) between control SN and ATDC SN from two-way ANOVA; *$p < 0.05$, **$p < 0.01$, ***$p < 0.001$.

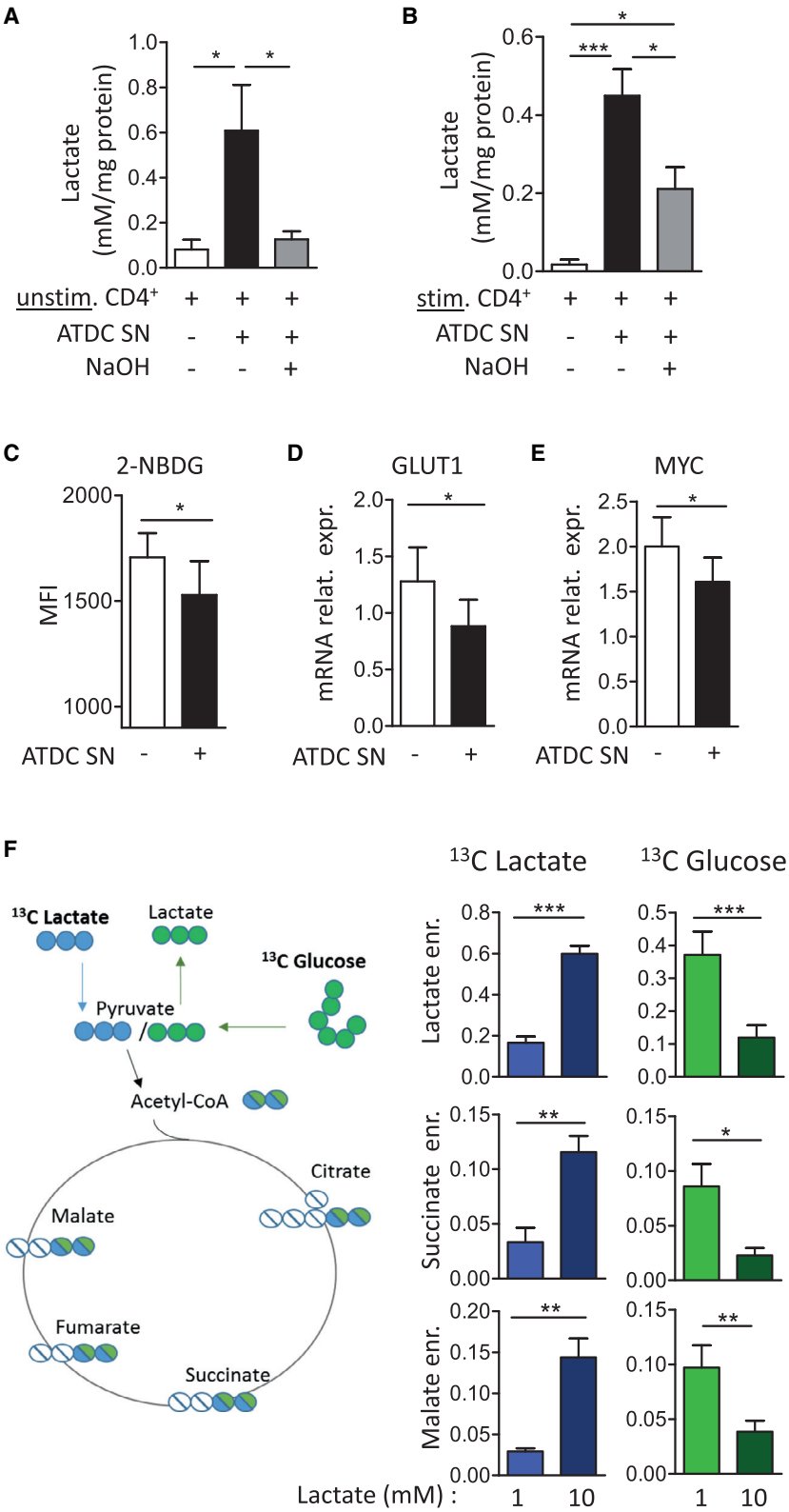

Figure 6. ATDC-Secreted Lactate Is Taken up by T Cells and Downregulates Their Glycolysis

(A–E) CD4$^+$ T cells were unstimulated (A) or stimulated (B–E) in absence or presence of ATDC SN or NaOH-neutralized ATDC SN.

(A and B) Intracellular lactate (n = 5 donors).

(C–E) Expressions of 2-NBDG (C, n = 6 donors), *GLUT1* (D, n = 18 donors), and *MYC* (E, n = 25 donors).

(F) Enrichments of metabolites in stimulated CD4$^+$ T cells incubated with ^{13}C lactate or with ^{13}C glucose in presence of 1–10mM lactate (n = 7 donors).

p values were calculated by one-way ANOVA in (A) and (B), and paired t tests were used in (C)–(F); *p < 0.05, **p < 0.01, ***p < 0.001.

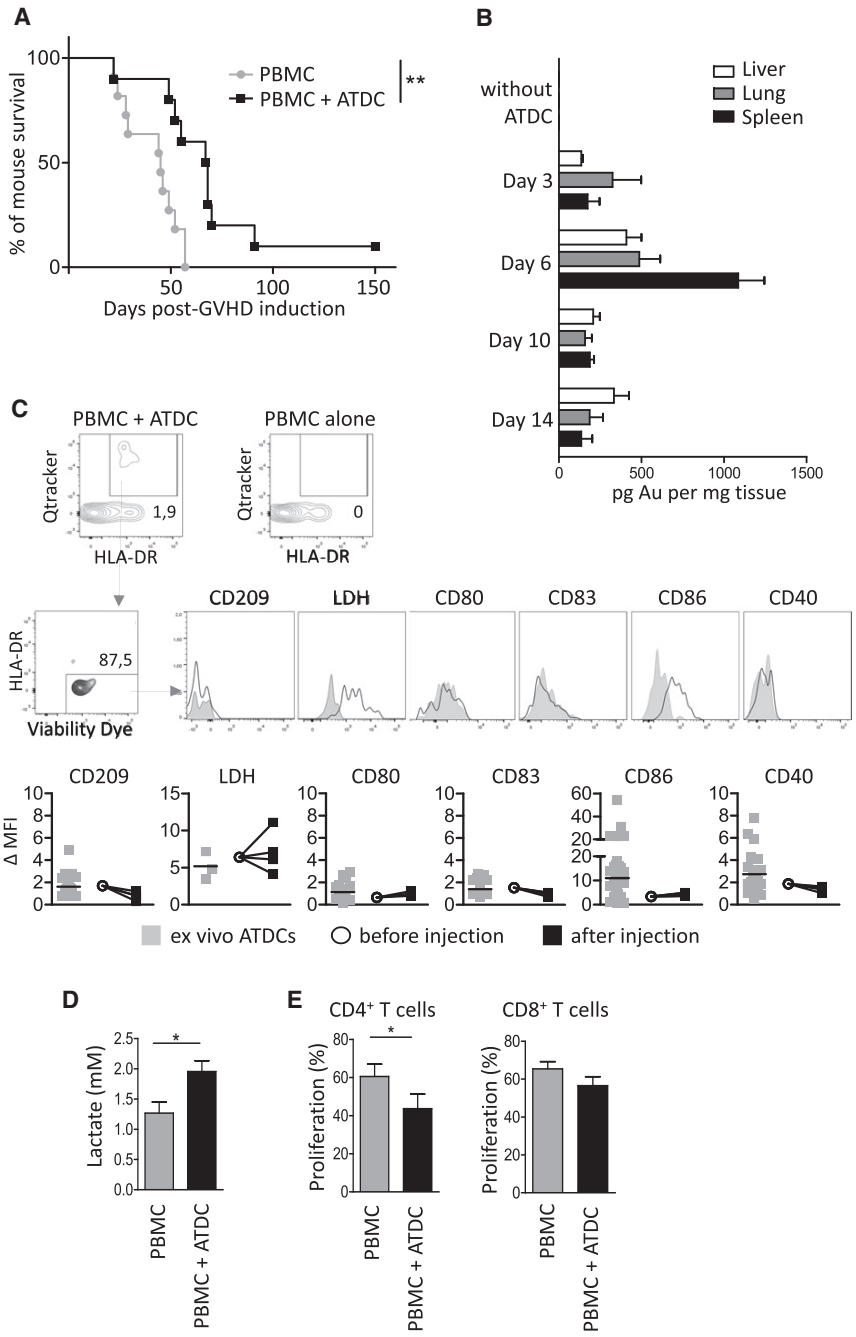

Figure 7. ATDCs Delay GVHD Development, Promote Increased Circulating Lactate, and Control T Cell Proliferation *In Vivo* in Humanized Mice

Irradiated NSG mice received PBMCs in absence or presence of autologous ATDCs.

(A) Survival curve displays mice survival. Median survivals are 45 days in PBMC group and 67.5 days in PBMC + ATDC group (n = 10–11 mice per group pooled from 3 experiments, log-rank [Mantel-Cox] test; **p ≤ 0.01).

(B) ATDCs were incubated with gold nanoparticles before injection. Bar graph depicts Au labeling per mg of tissue (n = 3 mice for day 3 and day 14; n = 5–6 mice from 2 experiments for the other conditions). See also Figures S5B–S5D.

(C) ATDCs were labeled with Qtracker and tracked in spleen 6 days later. Representative plots show the gating strategy, the viability, and the expression of markers by ATDCs (black line) and their respective isotype controls (gray shaded). Scatterplots depict the MFI marker/MFI isotype control ratios in ATDCs before or after injection (n = 4 mice for CD209 and LDH, and n = 5 mice for the other markers). Gray squares represent *ex vivo* ATDCs non-injected to mice (n ≥ 29 donors except for LDH, n = 3 donors). p values were calculated by unpaired t tests between *ex vivo* ATDCs (gray squares) and *in vivo* ATDCs (black squares). See also Figure S5E.

(D) Circulating lactate was measured at day 7 (n = 5 mice per group, unpaired t tests, *p ≤ 0.05).

(E) Mice were sacrificed at day 21, and splenocytes were stimulated with anti-CD3 and anti-CD28 for 3 days before proliferation assessment (n = 9 mice per group, unpaired t tests, *p ≤ 0.05).

transporters but also through acid-independent mechanisms. For instance, Gpr81 is a receptor of lactate reported to be expressed by immune cells, and its deletion was associated with a reduced differentiation of Tregs in mice (Ranganathan et al., 2018). Further proteomic, metabolomic, or lipidomic analyses will be instrumental in identifying other soluble factors, secreted or converted by ATDCs, which could participate in this immunosuppression.

Regarding the study of aerobic glycolysis and oxidative pathway in DCs, Malinarich et al. reported that human tolerogenic VitD3-Dex DCs display a higher glycolytic capacity and a higher mitochondrial respiration than do mature DCs (Malinarich et al., 2015). Here, using another protocol to derive human tolerogenic DCs, we confirmed these metabolic characteristics in comparison to immature MoDCs. The absence of IL-4 in ATDC generation is notably crucial to the suppressive properties of ATDCs and to their strong glycolytic capacity. IL-4 is a molecule known to induce PPARγ, a key regulator of lipid metabolism (Bouhlel et al., 2007). Further experiments will be required to understand how IL-4, currently used to differentiate different populations of tolerogenic DCs, modulates DC function and metabolic changes. In contrast to human DCs, increased glycolysis and lactate production observed after stimulation of murine DCs by TLR agonists have been associated with the acquisition of immunostimulatory functions (Everts et al., 2014). Following stimulation, these murine GM-CSF-derived DCs express iNOS and produce NO that inhibits OXPHOS and thus favors glycolysis (Everts et al., 2012). The involvement of iNOS is clearly different between murine and human DCs because our transcriptomic analysis revealed no overexpression of *INOS* in our ATDCs. Furthermore, iNOS inhibitor did not reverse the suppressive capacity of ATDCs. Regarding lactate on DCs, it has been reported that

human MoDCs stimulated with LPS and lactate produce less IL-12 as compared with MoDCs stimulated with LPS only (Gottfried et al., 2006; Nasi et al., 2013). We then postulate that lactate produced by ATDCs favors its own resistance to TLR-ligand stimulation. Further experiments will be necessary to investigate whether lactate contained in ATDC SN could influence the maturation and function of surrounding DCs.

Analysis of the ATDC phenotype and transcriptome indicates that ATDCs also shared some features with macrophages. Interestingly, lactate from the TME favors the polarization of anti-inflammatory M2-like tumor-associated macrophages (Colegio et al., 2014). However, initial studies reported that the metabolism of anti-inflammatory M2 macrophages was mainly based on OXPHOS fueled by fatty acid oxidation whereas inflammatory M1 macrophages displayed a glycolytic metabolism. Nevertheless, the requirement of fatty acid oxidation, as well as a potential role of glycolysis, in M2 polarization have been recently reconsidered (Divakaruni et al., 2018; Nomura et al., 2016; Wang et al., 2018).

Concomitantly to the phase I/II trial evaluating the safety of ATDCs, this study allowed us to decipher the mechanisms responsible for the tolerogenic activity of ATDCs, and it paves the way to the extension of their clinical application. Lactate-secreting cells, such as ATDCs, should be thus considered as an interesting therapeutic approach for immunosuppressive therapy but these results also raise fundamental questions about the involvement of these myeloid cells in the evasion of immune responses in the TME.

Limitations of Study

In vivo experiments indicated that ATDCs were able to delay GVHD in association with a transient increase of circulating lactate and a downregulation of $CD4^+$ T cell proliferative capacity. However, we could not formally prove that the increased circulating lactate observed in ATDC-treated mice was only due to ATDCs and that this elevated lactate was involved in *in vivo* effects of ATDCs. To demonstrate these two points, we sought to block LDH activity in ATDCs before injection. Unfortunately, ATDCs did not survive in presence of such inhibitors. One can speculate that ATDCs stimulate PBMCs to produce lactate *in vivo*. However, our *in vitro* results showed that ATDC-secreted lactate impaired T cell glycolytic activity (Figure 6). Finally, a role for lactate in controlling immune response to a transplant was recently shown. In this study, the injection of lactate was able to increase heart allograft survival in mice (Angelin et al., 2017).

STAR★METHODS

Detailed methods are provided in the online version of this paper and include the following:

- KEY RESOURCES TABLE
- LEAD CONTACT AND MATERIALS AVAILABILITY
- EXPERIMENTAL MODEL AND SUBJECT DETAILS
  - Healthy Volunteers
  - Xenogeneic GVHD Model
- METHOD DETAILS
  - Cell Generation
  - Antibodies and Flow Cytometry
  - T Cell Assays
  - Treg Expansion and Suppressive Ability
  - Metabolic Assay
  - IL-10 and IL-12 ELISAs
  - Lactacte/Glucose/ pH Measurements
  - ATP Measurement
  - RNA Extraction and Quantitative PCR
  - Agilent Microarray Hybridization
  - Confocal Microscopy
  - Mass Spectrometry Analyses on DCs and T Cells
  - Metabolomics and Lipidomics Analyses
  - *In Vivo* Experiments
- QUANTIFICATION AND STATISTICAL ANALYSIS
- DATA AND CODE AVAILABILITY
  - Microarray and Genomic Data Accession Numbers

SUPPLEMENTAL INFORMATION

Supplemental Information can be found online at https://doi.org/10.1016/j.cmet.2019.11.011.

ACKNOWLEDGMENTS

We thank DTC and MicroPicell facilities (Nantes University), as well as LABERCA facility (Oniris, Nantes). We also thank D. McIlroy and I. Anegon for critically reading the manuscript and S. Bezie for technical help. This work was funded by IMBIO-DC, the ONE Study (FP7-260687), and BIODRIM (FP7-305147). This work was also supported by IHU-CESTI (ANR-10-IBHU-005, Région Pays de la Loire and Nantes Métropole), ANR Jeunes Chercheurs (ANR-16-CE18-0001-01), DHU Oncogreffe, and LabexIGO (ANR-11-LABX-0016-01). We also thank the EU COST actions BM1305 and BM1404.

AUTHOR CONTRIBUTIONS

E.M., L.B.D., M.C.C., and A. Moreau conceived the project, designed the experiments, and wrote the manuscript. E.M., L.B.D., O.R., A.E., V.N.D., A. Managh, G. Bériou, J.A.H., N.O., C.P., A.A., and A. Moreau performed the experiments. E.M., L.B.D., C.L., M.G., T.P.V.M., E.C., X.P., M.C., E.K.G., B.A.L., B.V., G. Blancho, M.D., R.J., M.C.C., and A. Moreau analyzed the data.

DECLARATION OF INTERESTS

The authors declare no conflict of interest.

Received: October 29, 2018
Revised: July 17, 2019
Accepted: November 12, 2019
Published: December 3, 2019

REFERENCES

Angelin, A., Gil-de-Gómez, L., Dahiya, S., Jiao, J., Guo, L., Levine, M.H., Wang, Z., Quinn, W.J., 3rd, Kopinski, P.K., Wang, L., et al. (2017). Foxp3 reprograms T cell metabolism to function in low-glucose, high-lactate environments. Cell Metab. *25*, 1282–1293.e7.

Apicella, M., Giannoni, E., Fiore, S., Ferrari, K.J., Fernández-Pérez, D., Isella, C., Granchi, C., Minutolo, F., Sottile, A., Comoglio, P.M., et al. (2018). Increased lactate secretion by cancer cells sustains non-cell-autonomous adaptive resistance to MET and EGFR targeted therapies. Cell Metab. *28*, 848–865.e6.

Averous, J., Fonseca, B.D., and Proud, C.G. (2008). Regulation of cyclin D1 expression by mTORC1 signaling requires eukaryotic initiation factor 4E-binding protein 1. Oncogene *27*, 1106–1113.

Baas, M.C., Kuhn, C., Valette, F., Mangez, C., Duarte, M.S., Hill, M., Besançon, A., Chatenoud, L., Cuturi, M.C., and You, S. (2014). Combining autologous

dendritic cell therapy with CD3 antibodies promotes regulatory T cells and permanent islet allograft acceptance. J. Immunol. *193*, 4696–4703.

Bengtsson, H., Simpson, K., Bullard, J., and Hansen, K. (2008). aroma.affymetrix: a generic framework in R for analyzing small to very large Affymetrix data sets in bounded memory. Tech Report #745, Department of Statistics, University of California, Berkeley.

Bouhlel, M.A., Derudas, B., Rigamonti, E., Dièvart, R., Brozek, J., Haulon, S., Zawadzki, C., Jude, B., Torpier, G., Marx, N., et al. (2007). PPARgamma activation primes human monocytes into alternative M2 macrophages with anti-inflammatory properties. Cell Metab. *6*, 137–143.

Brand, A., Singer, K., Koehl, G.E., Kolitzus, M., Schoenhammer, G., Thiel, A., Matos, C., Bruss, C., Klobuch, S., Peter, K., et al. (2016). LDHA-associated lactic acid production blunts tumor immunosurveillance by T and NK cells. Cell Metab. *24*, 657–671.

Cao, W., Rosen, D.B., Ito, T., Bover, L., Bao, M., Watanabe, G., Yao, Z., Zhang, L., Lanier, L.L., and Liu, Y.J. (2006). Plasmacytoid dendritic cell-specific receptor ILT7-Fc epsilonRI gamma inhibits Toll-like receptor-induced interferon production. J. Exp. Med. *203*, 1399–1405.

Carpentier, S., Vu Manh, T.P., Chelbi, R., Henri, S., Malissen, B., Haniffa, M., Ginhoux, F., and Dalod, M. (2016). Comparative genomics analysis of mononuclear phagocyte subsets confirms homology between lymphoid tissue-resident and dermal XCR1(+) DCs in mouse and human and distinguishes them from Langerhans cells. J. Immunol. Methods *432*, 35–49.

Chakraborty, R., Mahendravada, A., Perna, S.K., Rooney, C.M., Heslop, H.E., Vera, J.F., Savoldo, B., and Dotti, G. (2013). Robust and cost effective expansion of human regulatory T cells highly functional in a xenograft model of graft-versus-host disease. Haematologica *98*, 533–537.

Chang, C.H., Curtis, J.D., Maggi, L.B., Jr., Faubert, B., Villarino, A.V., O'Sullivan, D., Huang, S.C., van der Windt, G.J., Blagih, J., Qiu, J., et al. (2013). Posttranscriptional control of T cell effector function by aerobic glycolysis. Cell *153*, 1239–1251.

Colegio, O.R., Chu, N.Q., Szabo, A.L., Chu, T., Rhebergen, A.M., Jairam, V., Cyrus, N., Brokowski, C.E., Eisenbarth, S.C., Phillips, G.M., et al. (2014). Functional polarization of tumour-associated macrophages by tumour-derived lactic acid. Nature *513*, 559–563.

Cuende, J., Liénart, S., Dedobbeleer, O., van der Woning, B., De Boeck, G., Stockis, J., Huygens, C., Colau, D., Somja, J., Delvenne, P., et al. (2015). Monoclonal antibodies against GARP/TGF-β1 complexes inhibit the immunosuppressive activity of human regulatory T cells in vivo. Sci. Transl. Med. *7*, 284ra56.

Divakaruni, A.S., Hsieh, W.Y., Minarrieta, L., Duong, T.N., Kim, K.K.O., Desousa, B.R., Andreyev, A.Y., Bowman, C.E., Caradonna, K., Dranka, B.P., et al. (2018). Etomoxir inhibits macrophage polarization by disrupting CoA homeostasis. Cell Metab. *28*, 490–503.e7.

Dray, S., and Dufour, A.B. (2007). The ade4 package: implementing the duality diagram for ecologists. J. Stat. Softw. *22*, 1–20.

Everts, B., Amiel, E., van der Windt, G.J., Freitas, T.C., Chott, R., Yarasheski, K.E., Pearce, E.L., and Pearce, E.J. (2012). Commitment to glycolysis sustains survival of NO-producing inflammatory dendritic cells. Blood *120*, 1422–1431.

Everts, B., Amiel, E., Huang, S.C., Smith, A.M., Chang, C.H., Lam, W.Y., Redmann, V., Freitas, T.C., Blagih, J., van der Windt, G.J., et al. (2014). TLR-driven early glycolytic reprogramming via the kinases TBK1-IKKε supports the anabolic demands of dendritic cell activation. Nat. Immunol. *15*, 323–332.

Faubert, B., Li, K.Y., Cai, L., Hensley, C.T., Kim, J., Zacharias, L.G., Yang, C., Do, Q.N., Doucette, S., Burguete, D., et al. (2017). Lactate metabolism in human lung tumors. Cell *171*, 358–371.e9.

Fischer, K., Hoffmann, P., Voelkl, S., Meidenbauer, N., Ammer, J., Edinger, M., Gottfried, E., Schwarz, S., Rothe, G., Hoves, S., et al. (2007). Inhibitory effect of tumor cell-derived lactic acid on human T cells. Blood *109*, 3812–3819.

Fox, J., and Weisberg, S. (2019). An {R} Companion to Applied Regression, Third Edition (SAGE Publications).

Gottfried, E., Kunz-Schughart, L.A., Ebner, S., Mueller-Klieser, W., Hoves, S., Andreesen, R., Mackensen, A., and Kreutz, M. (2006). Tumor-derived lactic acid modulates dendritic cell activation and antigen expression. Blood *107*, 2013–2021.

Goudot, C., Coillard, A., Villani, A.C., Gueguen, P., Cros, A., Sarkizova, S., Tang-Huau, T.L., Bohec, M., Baulande, S., Hacohen, N., et al. (2017). Aryl hydrocarbon receptor controls monocyte differentiation into dendritic cells versus macrophages. Immunity *47*, 582–596.e6.

Haniffa, M., Bigley, V., and Collin, M. (2015). Human mononuclear phagocyte system reunited. Semin. Cell Dev. Biol. *41*, 59–69.

Hannon, M., Lechanteur, C., Lucas, S., Somja, J., Seidel, L., Belle, L., Bruck, F., Baudoux, E., Giet, O., Chantillon, A.M., et al. (2014). Infusion of clinical-grade enriched regulatory T cells delays experimental xenogeneic graft-versus-host disease. Transfusion *54*, 353–363.

Hill, M., Thebault, P., Segovia, M., Louvet, C., Bériou, G., Tilly, G., Merieau, E., Anegon, I., Chiffoleau, E., and Cuturi, M.C. (2011). Cell therapy with autologous tolerogenic dendritic cells induces allograft tolerance through interferon-gamma and Epstein-Barr virus-induced gene 3. Am. J. Transplant. *11*, 2036–2045.

Hippen, K.L., Merkel, S.C., Schirm, D.K., Sieben, C.M., Sumstad, D., Kadidlo, D.M., McKenna, D.H., Bromberg, J.S., Levine, B.L., Riley, J.L., et al. (2011). Massive ex vivo expansion of human natural regulatory T cells (T(regs)) with minimal loss of in vivo functional activity. Sci. Transl. Med. *3*, 83ra41.

Hutchinson, J.A., Riquelme, P., Sawitzki, B., Tomiuk, S., Miqueu, P., Zuhayra, M., Oberg, H.H., Pascher, A., Lützen, U., Janssen, U., et al. (2011). Cutting Edge: Immunological consequences and trafficking of human regulatory macrophages administered to renal transplant recipients. J. Immunol. *187*, 2072–2078.

Johnson, W.E., Li, C., and Rabinovic, A. (2007). Adjusting batch effects in microarray expression data using empirical Bayes methods. Biostatistics *8*, 118–127.

Kim, S.H., Jung, H.H., and Lee, C.K. (2018). Generation, characteristics and clinical trials of ex vivo generated tolerogenic dendritic cells. Yonsei Med. J. *59*, 807–815.

Lutz, M.B., Suri, R.M., Niimi, M., Ogilvie, A.L., Kukutsch, N.A., Rössner, S., Schuler, G., and Austyn, J.M. (2000). Immature dendritic cells generated with low doses of GM-CSF in the absence of IL-4 are maturation resistant and prolong allograft survival in vivo. Eur. J. Immunol. *30*, 1813–1822.

Macedo, C., Turnquist, H.R., Castillo-Rama, M., Zahorchak, A.F., Shapiro, R., Thomson, A.W., and Metes, D. (2013). Rapamycin augments human DC IL-12p70 and IL-27 secretion to promote allogeneic type 1 polarization modulated by NK cells. Am. J. Transplant. *13*, 2322–2333.

Machen, J., Harnaha, J., Lakomy, R., Styche, A., Trucco, M., and Giannoukakis, N. (2004). Antisense oligonucleotides down-regulating costimulation confer diabetes-preventive properties to nonobese diabetic mouse dendritic cells. J. Immunol. *173*, 4331–4341.

Malinarich, F., Duan, K., Hamid, R.A., Bijin, A., Lin, W.X., Poidinger, M., Fairhurst, A.M., and Connolly, J.E. (2015). High mitochondrial respiration and glycolytic capacity represent a metabolic phenotype of human tolerogenic dendritic cells. J. Immunol. *194*, 5174–5186.

Managh, A.J., Edwards, S.L., Bushell, A., Wood, K.J., Geissler, E.K., Hutchinson, J.A., Hutchinson, R.W., Reid, H.J., and Sharp, B.L. (2013). Single cell tracking of gadolinium labeled CD4+ T cells by laser ablation inductively coupled plasma mass spectrometry. Anal. Chem. *85*, 10627–10634.

Managh, A.J., Hutchinson, R.W., Riquelme, P., Broichhausen, C., Wege, A.K., Ritter, U., Ahrens, N., Koehl, G.E., Walter, L., Florian, C., et al. (2014). Laser ablation-inductively coupled plasma mass spectrometry: an emerging technology for detecting rare cells in tissue sections. J. Immunol. *193*, 2600–2608.

Mansilla, M.J., Sellès-Moreno, C., Fàbregas-Puig, S., Amoedo, J., Navarro-Barriuso, J., Teniente-Serra, A., Grau-López, L., Ramo-Tello, C., and Martínez-Cáceres, E.M. (2015). Beneficial effect of tolerogenic dendritic cells pulsed with MOG autoantigen in experimental autoimmune encephalomyelitis. CNS Neurosci. Ther. *21*, 222–230.

Marín, E., Cuturi, M.C., and Moreau, A. (2018). Tolerogenic dendritic cells in solid organ transplantation: where do we stand? Front. Immunol. *9*, 274.

Merad, M., Sathe, P., Helft, J., Miller, J., and Mortha, A. (2013). The dendritic cell lineage: ontogeny and function of dendritic cells and their subsets in the steady state and the inflamed setting. Annu. Rev. Immunol. *31*, 563–604.

Monti, P., Mercalli, A., Leone, B.E., Valerio, D.C., Allavena, P., and Piemonti, L. (2003). Rapamycin impairs antigen uptake of human dendritic cells. Transplantation *75*, 137–145.

Moreau, A., Hill, M., Thébault, P., Deschamps, J.Y., Chiffoleau, E., Chauveau, C., Moullier, P., Anegon, I., Alliot-Licht, B., and Cuturi, M.C. (2009). Tolerogenic dendritic cells actively inhibit T cells through heme oxygenase-1 in rodents and in nonhuman primates. FASEB J. *23*, 3070–3077.

Moreau, A., Vandamme, C., Segovia, M., Devaux, M., Guilbaud, M., Tilly, G., Jaulin, N., Le Duff, J., Cherel, Y., Deschamps, J.Y., et al. (2014). Generation and in vivo evaluation of IL10-treated dendritic cells in a nonhuman primate model of AAV-based gene transfer. Mol. Ther. Methods Clin. Dev. *1*, 14028.

Mutis, T., van Rijn, R.S., Simonetti, E.R., Aarts-Riemens, T., Emmelot, M.E., van Bloois, L., Martens, A., Verdonck, L.F., and Ebeling, S.B. (2006). Human regulatory T cells control xenogeneic graft-versus-host disease induced by autologous T cells in RAG2-/-gammac-/- immunodeficient mice. Clin. Cancer Res. *12*, 5520–5525.

Nadig, S.N., Wieckiewicz, J., Wu, D.C., Warnecke, G., Zhang, W., Luo, S., Schiopu, A., Taggart, D.P., and Wood, K.J. (2010). In vivo prevention of transplant arteriosclerosis by ex vivo-expanded human regulatory T cells. Nat. Med. *16*, 809–813.

Nasi, A., Fekete, T., Krishnamurthy, A., Snowden, S., Rajnavölgyi, E., Catrina, A.I., Wheelock, C.E., Vivar, N., and Rethi, B. (2013). Dendritic cell reprogramming by endogenously produced lactic acid. J. Immunol. *191*, 3090–3099.

Nomura, M., Liu, J., Rovira, I.I., Gonzalez-Hurtado, E., Lee, J., Wolfgang, M.J., and Finkel, T. (2016). Fatty acid oxidation in macrophage polarization. Nat. Immunol. *17*, 216–217.

R Development Core Team (2005). R: A language and environment for statistical computing (R Foundation for Statistical Computing).

Ranganathan, P., Shanmugam, A., Swafford, D., Suryawanshi, A., Bhattacharjee, P., Hussein, M.S., Koni, P.A., Prasad, P.D., Kurago, Z.B., Thangaraju, M., et al. (2018). GPR81, a cell-surface receptor for lactate, regulates intestinal homeostasis and protects mice from experimental colitis. J. Immunol. *200*, 1781–1789.

Riquelme, P., Tomiuk, S., Kammler, A., Fändrich, F., Schlitt, H.J., Geissler, E.K., and Hutchinson, J.A. (2013). IFN-γ-induced iNOS expression in mouse regulatory macrophages prolongs allograft survival in fully immunocompetent recipients. Mol. Ther. *21*, 409–422.

Rosen, A.B., Kelly, D.J., Schuldt, A.J., Lu, J., Potapova, I.A., Doronin, S.V., Robichaud, K.J., Robinson, R.B., Rosen, M.R., Brink, P.R., et al. (2007). Finding fluorescent needles in the cardiac haystack: tracking human mesenchymal stem cells labeled with quantum dots for quantitative in vivo three-dimensional fluorescence analysis. Stem Cells *25*, 2128–2138.

See, P., Dutertre, C.A., Chen, J., Günther, P., McGovern, N., Irac, S.E., Gunawan, M., Beyer, M., Händler, K., Duan, K., et al. (2017). Mapping the human DC lineage through the integration of high-dimensional techniques. Science *356*, https://doi.org/10.1126/science.aag3009.

Segovia, M., Louvet, C., Charnet, P., Savina, A., Tilly, G., Gautreau, L., Carretero-Iglesia, L., Beriou, G., Cebrian, I., Cens, T., et al. (2014). Autologous dendritic cells prolong allograft survival through Tmem176b-dependent antigen cross-presentation. Am. J. Transplant. *14*, 1021–1031.

Segura, E., Touzot, M., Bohineust, A., Cappuccio, A., Chiocchia, G., Hosmalin, A., Dalod, M., Soumelis, V., and Amigorena, S. (2013). Human inflammatory dendritic cells induce Th17 cell differentiation. Immunity *38*, 336–348.

Shultz, L.D., Ishikawa, F., and Greiner, D.L. (2007). Humanized mice in translational biomedical research. Nat. Rev. Immunol. *7*, 118–130.

Søndergaard, H., Kvist, P.H., and Haase, C. (2013). Human T cells depend on functional calcineurin, tumour necrosis factor-α and CD80/CD86 for expansion and activation in mice. Clin. Exp. Immunol. *172*, 300–310.

Stoop, J.N., Robinson, J.H., and Hilkens, C.M. (2011). Developing tolerogenic dendritic cell therapy for rheumatoid arthritis: what can we learn from mouse models? Ann. Rheum. Dis. *70*, 1526–1533.

Tchao, N.K., and Turka, L.A. (2012). Lymphodepletion and homeostatic proliferation: implications for transplantation. Am. J. Transplant. *12*, 1079–1090.

Turnquist, H.R., Raimondi, G., Zahorchak, A.F., Fischer, R.T., Wang, Z., and Thomson, A.W. (2007). Rapamycin-conditioned dendritic cells are poor stimulators of allogeneic CD4+ T cells, but enrich for antigen-specific Foxp3+ T regulatory cells and promote organ transplant tolerance. J. Immunol. *178*, 7018–7031.

Walenta, S., Wetterling, M., Lehrke, M., Schwickert, G., Sundfør, K., Rofstad, E.K., and Mueller-Klieser, W. (2000). High lactate levels predict likelihood of metastases, tumor recurrence, and restricted patient survival in human cervical cancers. Cancer Res. *60*, 916–921.

Wang, F., Zhang, S., Vuckovic, I., Jeon, R., Lerman, A., Folmes, C.D., Dzeja, P.P., and Herrmann, J. (2018). Glycolytic stimulation is not a requirement for M2 macrophage differentiation. Cell Metab. *28*, 463–475.e4.

Wang, K., Lv, M., Chang, Y.J., Zhao, X.Y., Zhao, X.S., Zhang, Y.Y., Sun, Y.Q., Wang, Z.D., Suo, P., Zhou, Y., et al. (2019). Early myeloid-derived suppressor cells (HLA-DR$^{-/low}$CD33^{+}CD16^{-}) expanded by granulocyte colony-stimulating factor prevent acute graft-versus-host disease (GVHD) in humanized mouse and might contribute to lower GVHD in patients post allo-HSCT. J. Hematol. Oncol. *12*, 31.

Warburg, O., Wind, F., and Negelein, E. (1927). The metabolism of tumors in the body. J. Gen. Physiol. *8*, 519–530.

Woltman, A.M., de Fijter, J.W., Kamerling, S.W., van Der Kooij, S.W., Paul, L.C., Daha, M.R., and van Kooten, C. (2001). Rapamycin induces apoptosis in monocyte- and CD34-derived dendritic cells but not in monocytes and macrophages. Blood *98*, 174–180.

Zaitsu, M., Issa, F., Hester, J., Vanhove, B., and Wood, K.J. (2017). Selective blockade of CD28 on human T cells facilitates regulation of alloimmune responses. JCI Insight *2*, https://doi.org/10.1172/jci.insight.89381.

Zhang, W., Wang, G., Xu, Z.G., Tu, H., Hu, F., Dai, J., Chang, Y., Chen, Y., Lu, Y., Zeng, H., et al. (2019). Lactate is a natural suppressor of RLR signaling by targeting MAVS. Cell *178*, 176–189.e15.

STAR★METHODS

KEY RESOURCES TABLE

REAGENT or RESOURCE	SOURCE	IDENTIFIER
Antibodies		
anti-human CCR2 (CD192), dil:1/20	R&D systems	clone 48607, Cat#FAB151A; RRID: AB_357048
anti-human CCR5 (CD195), dil:1/20	BD Biosciences	clone 2D7/CCR5, Cat#556903; RRID: AB_398619
anti-human CCR7 (CD197), dil:1/20	BD Biosciences	clone 3D12, Cat#557648; RRID: AB_396765
anti-human CCR9 (CD199), dil:1/20	R&D systems	clone 112509, Cat#FAB179A; RRID: AB_357088
anti-human CD11b, dil:1/50	Beckman Coulter	clone BEAR1, Cat#IM0530; RRID: AB_130987
anti-human CD11c, dil:1/100	BD Biosciences	clone S-HCL-3, Cat#333144; IVD
anti-human CD123, dil:1/20	BD Biosciences	clone 9F5, Cat#551065; RRID: AB_394029
anti-human CD127, dil:1/50	BD Biosciences	clone hIL-7R-M21, Cat#557938; RRID: AB_2296056
anti-human CD14, dil:1/100	BD Biosciences	clone M5E2, Cat#557742; RRID: AB_396848
anti-human CD141, dil:1/20	BD Biosciences	clone 1A4, Cat#559781; RRID: AB_397322
anti-human CD1a, dil:1/50	BD Biosciences	clone HI149, Cat#555808; RRID: AB_396142
anti-human CD1c, dil:1/25	Thermo Fisher Scientific	clone L161, Cat#46-0015-42; RRID: AB_10548936
anti-human CD20, dil:1/20	BD Biosciences	clone 2H7, Cat#556633; RRID: AB_396502
anti-human CD206, dil:1/50	BD Biosciences	clone 19.2, Cat#551135; RRID: AB_394065
anti-human CD209, dil:1/50	BD Biosciences	clone DCN46, Cat#551265; RRID: AB_394123
anti-human CD25, dil: 1/50	BD Biosciences	clone M-A251, Cat#557753, Cat#555431, Cat#555434; RRID: AB_396859, RRID: AB_395825, RRID: AB_398598
anti- human CD28, 1μg/mL	BD Biosciences	clone 28.2, Cat#555726; RRID: AB_396069
anti-human CD3, dil:1/50	BD Biosciences	clone UCHT1, Cat#555332, Cat#555333; RRID: AB_395739, RRID: AB_395740
anti- human CD3, 1μg/mL	European Collection of Authenticated Cell Culture	clone OKT3, Cat# 86022706; RRID: CVCL_2665
anti-human CD4, dil:1/50	BD Biosciences	clone RPA-T4, Cat#555346, Cat#555347, Cat#560650; RRID: AB_395751, RRID: AB_395752, RRID: AB_1727476
anti-human CD40, dil:1/50	BD Biosciences	clone 5C3, Cat#555588; RRID: AB_395963
anti-human CD45, dil:1/50	BD Biosciences	clone HI30, Cat#557748; RRID: AB_396854
anti-human CD56, dil:1/12	BD Biosciences	clone B159, Cat#557711; RRID: AB_396820
anti-human CD64, dil:1/25	BD Biosciences	clone 10.1, Cat#555527; RRID: AB_395913
anti-human CD80, dil:1/300	BD Biosciences	clone L307.4, Cat#561134; RRID: AB_10565974
anti-human CD83, dil:1/100	BD Biosciences	clone HB15e, Cat#551058; RRID: AB_394025
anti-human CD86, dil:1/50	BD Biosciences	clone 2331, Cat#555660; RRID: AB_398608
anti-human CX3CR1, dil:1/20	Thermo Fisher Scientific	clone 2A9.1, Cat#17-6099-42; RRID: AB_11149136
anti-human FcεR1, dil:1/20	Thermo Fisher Scientific	clone AER-37, Cat#25-5899-42; RRID: AB_2573495
anti-human FoxP3, dil:1/15	Thermo Fisher Scientific	clone PCH101, Cat#45-4776-42; RRID: AB_10854725
anti-human HLA-DR, dil:1/100	BD Biosciences	clone G46-6, Cat#561225; RRID: AB_10584333
anti-human HLA-G, dil:1/200	Thermo Fisher Scientific	clone 87G, Cat#17-9957-42; RRID: AB_10671139
anti-human IFN-γ, dil:1/100	BD Biosciences	clone B27, Cat#557995; RRID: AB_396977
anti- human IL10, dil:1/50	BD biosciences	clone JES3-9D7, Cat#554495; RRID: AB_395432
anti-human IL-17A, dil:1/50	Thermo Fisher Scientific	clone eBio64DEC17, Cat#17-7179-42; RRID: AB_1582221
anti-human ILT2 (CD85j), dil:1/50	Miltenyi Biotech	clone GHI/75, Cat#130-101-552; RRID: AB_2659386
anti-human ILT3 (CD85k), dil:1/50	BD Biosciences	clone ZM3.8, Cat#564181; RRID: AB_2738649
anti-human ILT4 (CD85d), dil:1/50	R&D systems	clone 287219, Cat#FAB2078N
anti-human ILT7 (CD85 g), dil:1/20	BD Biosciences	clone 17G10.2, Cat#562340; RRID: AB_10893797

(*Continued on next page*)

Continued

REAGENT or RESOURCE	SOURCE	IDENTIFIER
anti-human LDH, dil:1/200	Abcam	Cat#Ab9002; RRID: AB_306930
anti-human PDL-1 (CD274), dil:1/20	BD Biosciences	clone MIH1, Cat#558065; RRID: AB_647176
anti-human TNFα, dil:1/50	BD Biosciences	Clone 6401.1111, Cat#340511; RRID: AB_400434
anti-mouse CD45, dil:1/500	BD Biosciences	clone 30-F11, Cat#550994; RRID: AB_394003
anti-sheep IgG(H+L), dil:1/80	Jackson ImmunoResearch	Cat#713-095-147; RRID: AB_2340719
Biological Samples		
Healthy adult blood	French Blood Service, Nantes, France	N/A
Chemicals, Peptides, and Recombinant Proteins		
GM-CSF	CellGenix	Cat#1412-050
IL-4	CellGenix	Cat#1403-050
Rapamycin	Sigma	Cat#553210-100UG
LPS	Sigma	Cat#L4391-1MG
Human recombinant IFN-γ	R&D systems	Cat#285-IF-100
Cell proliferation Dye	ebioscience	Cat#65-0840, Cat#65-0842
Thymidine, [Methyl-3H]	Perkin Elmer	Cat#NET027A005MC
2-NBDG	Thermo Fisher Scientific	Cat#N13195
CCCP	Sigma	Cat# C2920
Oligomycin	Sigma	Cat# 75351
Rotenone	Sigma	Cat# R8875
Antimycin A	Sigma	Cat# A8674
Etomoxir sodium salt hydrate	Sigma	Cat# E1905
2-Deoxy-D-glucose	Sigma	Cat# D8375
Glucose	GIBCO	Cat#A2494001
Glutamine	GIBCO	Cat#25030081
Pyruvate	Sigma	Cat# S8336
HCl	VWR	Cat#20252-290
Sodium L-lactate	Sigma	Cat#L7022
Aminoguanidine hemisulfate salt	Sigma	Cat#A7009
1-Methyl-D-tryptophan	Sigma	Cat#452483
Phorbol 12-myristate 13-acetate	Sigma	Cat#8139-5MG
Ionomycin	Sigma	Cat#I9657-1MG
BrefeldinA	Sigma	Cat#B7651-5MG
Viability Dye	Thermo Fisher Scientific	Cat#65-0866
DAPI	Thermo Fisher Scientific	Cat#62247
Human recombinant IL-2	Novartis	34009 562 158 6 7
13C-Glucose	Cambridge isotope laboratories	CLM-1396
13C-Lactate	Cambridge isotope laboratories	CLM-1579
Qtracker	Thermo Fisher Scientific	Cat#Q25001MP
Collagenase D	Sigma	Cat#11088866001
NaOH	Sigma	Cat#795429
Gold nanoparticles	Sigma	Cat#753645
FOXP3/Transcription factor staining buffer set	Thermo Fisher Scientific	Cat#.00-5523-00
Critical Commercial Assays		
Human monocyte isolation kit II	MiltenyiBiotec	Cat#130-091-153
Human CD4+ T cell isolation kit	MiltenyiBiotec	Cat#130-096-533
Human CD25+ isolation kit	MiltenyiBiotec	Cat#130-092-983
Human Pan T cell isolation kit	MiltenyiBiotec	Cat#130-096-535

(*Continued on next page*)

Continued

REAGENT or RESOURCE	SOURCE	IDENTIFIER
Human IL-10 ELISA BD OptEIA	BD Biosciences	Cat#555157
Human IL-12p70 ELISA BD OptEIA	BD Biosciences	Cat#559258
Reagent Cobas Integra LDH	Roche	Cat#30047321211
ATPLite Luminescence ATP detection assay system	PerkinElmer	Cat#6016941
RNeasy mini kit	QIAGEN	Cat#74106
Fast SYBR Green MasterMix	Thermo Fisher Scientific	Cat#438618
Micro BCA Protein assay kit	Thermo Fisher Scientific	Cat#23235
Seahorse XF- Palmitate BSA FAO substrate kit	Agilent	Cat#102720-100
Deposited Data		
ATDCs, MoDCs and rMoMacro microarrays	NCBI GEO	GEO: GSE104438
Experimental Models: Organisms/Strains		
NOD-SCID-*IL2rg*$^{-/-}$	Charles River	Strain code: 614
Oligonucleotides		
Primers for*PDK1, PDK4, HPRT, GLUT1, MYC, IFNG, TNFA, CCND1, FOXP3, MCT1*, see Table S3	This paper	N/A
Software and Algorithms		
FlowJo VX	FlowJo	https://www.flowjo.com/
GraphPad Prism V5	Graphpad Software	https://www.graphpad.com/
FIJI running ImageJ, version 1.52p	ImageJ	http://imagej.net/
Seahorse Wave 2.4	Agilent	https://www.agilent.com/
R software	R Development Core Team, 2005	https://www.r-project.org
aroma.affymetrix	Bengtsson et al., 2008	http://www.aroma-project.org/
sva package	Johnson et al., 2007	https://bioconductor.org/packages/release/bioc/html/sva.html
ade4 package	Dray and Dufour, 2007	http://pbil.univ-lyon1.fr/ADE-4
car package	Fox and Weisberg, 2019	https://cran.r-project.org/web/packages/car/index.html
Gene-E	Broad Institute	https://software.broadinstitute.org/GENE-E/
MassLynx	Waters Corporation	https://www.waters.com/waters/home.htm
Target Lynx	Waters Corporation	https://www.waters.com/waters/home.htm
Xcalibur V2.2	ThermoScientific	https://www.thermofisher.com/
Other		
AIMV medium	Thermo Fisher Scientific	Cat#0870112-DK
RPMI 1640 Medium	Thermo Fisher Scientific	Cat#11875093
RPMI 1640 Medium, no glucose	Thermo Fisher Scientific	Cat#11879020
Glucose –test strips	NOVA Biomedical	Cat#42214
Lactate- test strips	NOVA Biomedical	Cat#47486

LEAD CONTACT AND MATERIALS AVAILABILITY

Further information and requests for resources and reagents should be directed and will be fulfilled by the Lead Contact, Aurélie Moreau (aurelie.moreau@univ-nantes.fr). This study did not generate new unique reagents.

EXPERIMENTAL MODEL AND SUBJECT DETAILS

Healthy Volunteers

Human blood cells from healthy volunteer donors (French Blood Service, Nantes, France) were used in this project. Blood collection at French Blood Service is regulated by the Order of 5th April 2016 relating to blood donors screening criteria. An agreement transfer

exists between French Blood service and the CRTI laboratory. Around 270 blood samples were used in this study and all donors (mixed, men and women; 18-65 years old) gave their informed consent.

Xenogeneic GVHD Model

8-12 weeks old male NOD/SCID/*Il2rg*$^{-/-}$ mice (Charles River) bred in the Labex IGO humanized rodent facility were used in this study. Mice were exposed to a conditioning dose of 1.5 Gray of whole-body gamma irradiation and then received 5x10^6 thawed PBMCs and 5x10^6 autologous ATDCs simultaneously by IV route on the same day. Animals that displayed a reduction greater than 20% total of body weight were sacrificed according to the local ethical committee guidelines. These experiments performed in mice were carried out in strict accordance with the protocol approved by the Commitee on the Ethics of Animal Experiments of Pays de la Loire. Mice were housed under specific pathogen-free conditions (health status checked every three months) and classical husbandry conditions (12 h-light/dark cycles, 21 ± 1°C and standard chow diet (Safe, A04-10, U8221G10R)).

METHOD DETAILS

Cell Generation

Dendritic cells were generated from monocytes isolated from healthy volunteer donors. Monocytes were isolated either by elutriation of PBMCs (Clinical Development and Transfer Platform, Nantes, France) or by magnetic labeling (untouched cells, Human monocyte Isolation kit II). ATDCs were differentiated following a 6 day-culture of 2.5 × 10^6 monocytes in 5ml of AIMV medium CTS supplemented with recombinant human GM-CSF at 100U/mL in a 6-well plate. To obtain MoDC, 2.5x10^6 monocytes were incubated in a 6-well plate in 5 mL of complete medium (RPMI 1640 medium containing 10% Fetal Calf serum (FCS), 1% L-glutamin, 1% antibiotics, 1mM Sodium Pyruvate, 1mM HEPES, 1% non-essential amino acids) supplemented with recombinant human IL-4 (200U/mL) and recombinant human GM-CSF (100U/mL) for 6 days. ATDC + IL-4 were differentiated in AIMV medium supplemented with recombinant human GM-CSF (100U/mL) and IL-4 (200U/mL). iRapa-DCs were initially differentiated similarly to MoDCs and rapamycin (10ng/mL) was then added to the medium at day 2 and 4. LDH activity was measured in DCs using the Roche diagnostic kit on a Cobas 8000 device (Roche Diagnostics, Mannheim DE) according to the manufacturer's protocol. This assay is based on the measure of NADH appearance after transformation of lactate from pyruvate by LDH.

ATDC and MoDC SN were obtained following cultures of DCs (0.25 x10^6 cells/mL) in complete RPMI medium. After 6 days, supernatants were collected and frozen at −80°C until use. In some experiments, supernatants were filtrated to 3-KDa filters (VWR) and both fractions were tested in MLR assay.

Mature DCs were obtained after a 48 h stimulation of MoDC with LPS at 1μg/mL. To evaluate the maturation resistance, DCs (either ATDCs or MoDCs) were cultured 48 h in a 96-well plate at 0.5x10^5 cells/well or in a 24-well plate at 1x10^6 cells/well in complete medium in presence of LPS (200ng/mL) alone or LPS and IFN-γ (50ng/mL).

DCs were generated from mixed donors (men and women) and all DC cultures were performed at 37°C with 5% CO_2.

Antibodies and Flow Cytometry

Antibodies used in this study are listed in Key Resources Table. For intracellular staining, cells were stained then fixed/permeabilized according to the ThermoFisher protocol. Permeabilized cells were incubated in Perm. Buffer with anti-IFN-γ, IL-17A or appropriate isotype control (with human sera). Foxp3 and LDH stainings were performed according to the Foxp3 manufacturer's protocol. LDH staining was revealed using a FITC-coupled anti-sheep IgG(H+L) secondary antibody. For glucose intake assay, cells were incubated with 200 μM 2-NBDG diluted in free glucose medium RPMI 1640 medium (+) L-Glutamine, (-) D-Glucose, for 30 min at 37°C and 5% of CO_2. For the detection of intracellular cytokines, PMA (50ng/mL), ionomycin (1μM) and brefeldinA were added for 5 h before staining. Dead cells were excluded using DAPI or Fixable Viability Dye eFluor450 or eFluor506. Flow cytometry was performed on a FACS Canto II or a FACS LSR (BD Biosciences) and analyzed with FlowJo software.

T Cell Assays

For MLR assay, allogeneic CD3$^+$ T cells were isolated using a pan T cell isolation kit and cultured in 96-well plates with DCs at different ratios. T cells were labeled with Cell Proliferation Dye (CPD) and T cell proliferation was measured after 5 days by CPD dilution by flow cytometry.

To investigate the suppressive function of ATDCs, autologous CD4$^+$ T cells were selected using a CD4$^+$ T Cell isolation kit II and CD4$^+$CD25$^-$ cells were selected following an additional depletion of CD25$^+$ cells using a CD25$^+$ isolation kit. In most of the experiments, T cells were labeled with Cell Proliferation Dye (CPD) efluor450 and cultured in 96-well plates with DC (ATDCs or MoDCs) at a 1:1 ratio and with mature DCs at a 1:0.1 ratio for 6 days. In Figure 4C, proliferation was assessed by the addition of 1μCi ^{3}H-thymidine/well for the last 8 h. In some experiments, supernatants from MLR in the presence or absence of ATDCs were collected. These supernatant were then frozen at −80°C until use. A volume of 100μL of supernatants was added to a new assay to test suppressive activity. The neutralization of supernatants was performed by addition of NaOH to a final concentration of 5 mM. In other experiments, transwells (3 μm pore size, Corning) were added to the well to define whether contact dependent mechanisms occurred. In some experiments, Glucose, Glutamine, Pyruvate, HCl or NaLactate were added to the medium. In other assays, inhibitors of iNOS (Aminoguanonidine, 100 μM) and IDO (1-Methyl-D-tryptophan, 20μM) or anti-IL10 antibody (clone JES3-9D7, 10μg/mL) or anti-TGF-β (clone 2GT, 2μg/mL) were added in the suppressive assay.

Anti-CD3/anti-CD28 Stimulation

$CD4^+$ purified T cells ($5x10^5$ cells) were stimulated with 1μg/mL of anti-CD3 (OKT3 clone), 1μg/mL of anti-CD28 (28.6 clone) in 48 well-plate for 5 days at 37°C and 5% CO_2. ATDC SN was added at day 0 and represented 50% of the final medium volume.

PMA-Ionomycin Stimulation

$CD4^+$ purified T cells ($5x10^5$ cells) were cultured in 96 well-plate overnight before the stimulation with Phorbol 12-Myristate 13-acetate (PMA) and ionomycin in presence or absence of ATDC SN for 5 h.

T cells were isolated from mixed donors (men and women) and all T cell cultures were performed at 37°C with 5% CO_2.

Treg Expansion and Suppressive Ability

$CD4^+CD25^+CD127^-$ T cells were purified by cell sorter (ARIAII, BD Biosciences) and $3x10^5$ cells were stimulated with 1mg/mL of anti-CD3 (OKT3 clone), 1mg/mL of anti-CD28 (28.6 clone) and 1000U/mL of IL-2 (Proleukin) for 14 days in 48 well plates. Medium was replaced at day 7. ATDC SN was added at day 0 and day 7 and represented 50% of the final medium volume. To evaluate their suppressive ability, expanded Tregs (1.25; 2.5 or $5x10^5$ cells) were cultured with autologous purified CPD-labeled $CD4^+CD25^-$ T cells ($5x10^5$ cells) and mature DCs ($5x10^4$ cells). T cell proliferation was evaluated 6 days later by CPD dilution. Treg were isolated from mixed donors (men and women) and Treg expansion and assays were performed at 37°C with 5% CO_2.

Metabolic Assay

ATDC or MoDC were plated on Seahorse Bioanalyzer XFe24 or XFp culture plates (120.000 or 100 000 cells/well respectively) in Seahorse XF-base medium supplemented with 9mM of glucose, 0,86mM of NaOH, 1mM of pyruvate and 2mM of glutamine. Before the experiment, cells were incubated 20 min at 37°C and 0% CO_2. Drugs used during the plate reading were CCCP (2,5μM), oligomycin (2,5 μM), Rotenone (1μM), Antimycin A (1μM), Etomoxir (50μM) and 2-DG (100mM). Palmitate oxidation assay was performed using Agilent Seahorse XF Palmitate-BSA FAO substrate kit according to manufacturing protocol. OCAR and ECAR readouts were obtained using Seahorse XF24 analyzer. Seahorse data analysis was performed using Seahorse Wave 2.4 software. Glycolytic capacity was calculated as ((Glucose – basal)x100)/(oligomycin-basal), basal respiration was calculated as basal-antimycin, ATP linked respiration was calculated as basal – oligomycin and maximal respiration was calculated as FCCP – antimycin.

IL-10 and IL-12 ELISAs

To measure IL-10 and IL-12p70 production after LPS/IFNγ stimulation, culture supernatant of unstimulated and stimulated ATDCs and MoDCs were harvested after 48 h. Level of these cytokines was determined by capture ELISA according to the manufacturer's instructions.

Lactacte/Glucose/ pH Measurements

Glucose and lactate were quantified from supernatants of DC cultures and from MLR in presence or not of ATDC with Glu – Test strips and Lac – Test strips respectively. pH was measured in supernatants of DC cultures with HANNA pH210 microprocessor pH meter at room temperature.

ATP Measurement

ATDC or MoDC were plated on flat bottom 96 wells plate (50.000 cells/well) in complete media. Intracelullar ATP was measured using ATPlite Luminescence ATP Detection Assay System according to manufacturer protocol. Luminescence was measured with a SPARK 10M (TECAN) plate reader.

RNA Extraction and Quantitative PCR

Total RNA from cell cultures was extracted with RNeasy mini kit according to manufacturer protocol. mRNA were reverse transcribed into first strand cDNA using poly dT oligonucleotide and Moloney murine leukemia virus reverse transcriptase (Invitrogen). Real-time quantitative PCR was performed in a ViiA7 Real-Time PCR system (Thermofisher) Detection System using Fast SYBR Green master mix. The oligonucleotides used are listed on Table S3. Relative expression was calculated with the $2^{-\Delta\Delta Ct}$ method.

Agilent Microarray Hybridization

Transcriptomic analysis was performed on ATDCs, MoDCs and rMoMacro. The Agilent data have been deposited in GEO (GEO: GSE104438). In the microarray experiments, $CD14^+$ sorted monocytes from 6 different donors were used to differentiate ATDCs, MoDCs and rMoMacro from the same samples. ATDCs were generated as described in cell generation section, whereas MoDCs were cultured for 6 days in IMDM medium (Invitrogen) supplemented with 10% FBS (Gemini), 1000 U/mL rhGM-CSF (Miltenyi), 1000 U/mL rhIL-4 (Miltenyi) at a concentration of $0,5x10^6$ cells/mL. rMoMacro were obtained following a 7 day-culture of 1×10^6 monocytes in 3 mL of RPMI 1640 medium supplemented with 10% FCS (Biochrom), 2 mM Glutamax (Invitrogen), 100 U/mL penicillin-100 ug/mL streptomycin, and 100ng/mL rhM-CSF (R&D) in 6-well plate. RNA were extracted from cultured cells using the RNeasy Plus Mini kit and then labeled and hybridized on Agilent whole genome oligo Microarrays (8x60K) according to the ''One-Color Microarray-Based Gene Expression Analysis'' protocol (Agilent) (Riquelme et al., 2013). Background corrected intensity values were quantile normalized and log2 transformed. Gene Set Enrichment Analysis (GSEA) was performed on ATDCs and MoDCs using the lists of hallmark gene sets from the Molecular Signature Database (http://software.broadinstitute.org/gsea/downloads.jsp) using default

parameters. Core enrichment genes corresponding to those contributed the most to the observed enrichment were extracted from GSEA and their differential expression was represented as heatmaps using GENE-E software.

Based on the common genes, these expression datas were then combined with public Affymetrix microarray datasets obtained from human monocytes, and from *in vitro*- and *in vivo*- differentiated DCs and macrophages (GEO: GSE40484, GSE102046) (Goudot et al., 2017). Affymetrix HuGene1.1 ST raw data files were normalized by the robust multiarray average (RMA) algorithm and summarized, after background correction, using the R package *aroma.affymetrix* (Bengtsson et al., 2008; R Development Core Team, 2005). The Agilent and Affymetrix processed datasets were matched using gene symbol as primary identifier. The Agilent gene expression data was then adjusted to the Affymetrix one using the ComBat function of the *sva* package (Johnson et al., 2007), as done in Carpentier et al. (2016). Principal Component Analysis (PCA) was performed as described in Goudot et al. (2017) in order to compare all the above myeloid subsets within each other. Briefly, we used the dudi.pca function of the *ade4* package (Dray and Dufour, 2007) and ellipses were drawn using the dataEllipse function of the *car* package (Fox and Weisberg, 2019) with the level parameter set at 0.5.

Confocal Microscopy

ATDC and MoDC were stained with Bodipy and then fixed with Prolong Gold with DAPI. Confocal microscopy was performed using A1 R Si Confocal Microscope (Nikon, France). Image analysis was performed using Fiji software.

Mass Spectrometry Analyses on DCs and T Cells

Absolute Quantification of Metabolites

Lactate, citrate, succinate, fumarate and malate were analyzed by liquid chromatography-tandem mass spectrometry (LC-MS/MS) in serum or cell lysate samples. All solvents were LC-MS grade and purchased from Biosolve. Standard compounds were obtained from Sigma Aldrich. A pool of reference standard solutions was prepared and serially diluted in water to obtain 7 standard solutions ranging 0.1-100 μmol/L. $CD4^+$ purified T cells ($2{,}5x10^6$ cells) were incubated overnight before their stimulation with PMA/ionomycin in presence or absence of ATDC SN for 5 h. After stimulation cells were washed twice at 4°C and frozen in liquid nitrogen. Cells were then lysed with distilled water and centrifugated. One part of supernatants was used for protein quantification with bicinchoninic acid assay kit according to supplier's instructions and the other part was used for metabolite quantification. Briefly, exogenous ^{13}C-metabolite labeled internal standards were added and supernatants were deproteinized by adding 4:1 methanol and then centrifuged. Supernatants were recovered and dried using nitrogen stream. Finally, dried samples were solubilized in water containing 0.1% formic acid and then injected into the LC-MS/MS system. LC–MS/MS analyses were performed on a Xevo TQD mass spectrometer with an electrospray (ESI) interface and an Acquity H-Class UPLC device (Waters Corporation, Milford, USA). Samples (10 μL) were injected onto a UPLC BEH C_{18} column (2.1 × 100 mm i.d., 1.7 μm particle size; Waters Corporation) held at 35°C, and compounds were separated with a linear gradient of mobile phase B (100% ACN, 0.1% formic acid) in mobile phase A (5% ACN, 0.1% formic acid) at a flow rate of 400 μL/min. Mobile phase B was kept constant for 1 min at 1%, linearly increased from 1% to 90% for 5 min, kept constant for 1 min, returned to the initial condition over 0.5 min, and kept constant for 1.5 min before the next injection. Targeted compounds were then detected by the mass spectrometer with the ESI interface operating in the negative ion mode (capillary voltage, 2.5 kV; desolvatation gas (N_2) flow and temperature, 900 L/h and 450°C; source temperature, 150°C). The multiple reaction monitoring (MRM) mode was applied for MS/MS detection as detailed below. Chromatographic peak area ratios between unlabeled compounds and their respective internal standards constituted the detector responses. Standard solutions were used to plot calibration curves for quantification. Data acquisition and analyses were performed with MassLynx and TargetLynx (+ IsoCor) softwares, respectively. Metabolite concentrations in cell lysates were normalized with total protein contents of samples.

Compound	MRM (*m/z*)	Cone (V)	Collision (eV)
Citrate	190,9 → 110,9	25	15
$^{13}C_2$-citrate	192,9 → 111,9	25	15
Fumarate	114,9 → 70,9	20	10
$^{13}C_2$-fumarate	116,9 → 71,9	20	10
Lactate	88,93 → 44,9	30	15
$^{13}C_3$-lactate	91,94 → 45,9	30	12
Malate	132,9 → 114,9	25	15
^{13}C-malate	133,9 → 115,9	25	15
Pyruvate	86,9 → 42,9	20	12
^{13}C-pyruvate	87,9 → 43,9	20	12
Succinate	116,9 → 72,9	25	15
d_4-succinate	120,9 → 76,9	25	15

Glucose and Lactate Tracking

For glucose tracking in ATDCs and MoDCs, cells were cultured in DMEM supplemented with 1mM of pyruvate, 2mM of glutamine and 9mM of ^{13}C-Glucose for 24 h. For glucose and lactate tracking experiments in CD4$^+$ T cells, cells were stimulated with PMA and ionomycin for 5 h in DMEM medium supplemented with 1mM of pyruvate and 2mM of glutamine and 9 mM of ^{12}C- or ^{13}C-glucose and 1mM or 10mM of ^{12}C- or ^{13}C lactate. Carbon isotope tracing was quantified in samples (prepared as described above) by liquid chromatography-high resolution mass spectrometry (LC-HRMS). LC-HRMS analyses were performed on a Synapt G2 HRMS Q-TOF mass spectrometer equipped with an ESI interface operating in the negative mode and an Acquity H-Class UPLC device (Waters Corporation). Compounds were separated as described above and the full-HRMS mode was applied for detection (*m/z* range 50-600) at a mass resolution of 25,000 full-widths at half maximum. The ionization settings were as follows: capillary voltage, −1 kV; cone voltage, 30 V; desolvation gas (N_2) flow rate, 900 L/h; desolvation gas/source temperatures, 550/120°C. Leucine enkephalin solution (2 μg/mL, 50% acetonitrile) was infused at a constant flow rate of 10 μL/min in the lockspray channel, allowing for correction of the measured *m/z* throughout the batch (theoretical *m/z* 554.2658 in negative mode). Data acquisition and processing were achieved using MassLynx and TargetLynx softwares. Both labeled and unlabeled compounds were detected by their calculated exact theoretical *m/z* with a mass tolerance of ± 0.001 Da. Enrichments were then deducted as follow: M+3 count peak area for lactate or M+2 area for malate and succinate / total relative amount of lactate, malate or succinate respectively.

Metabolomics and Lipidomics Analyses

Supernatants were obtained from ATDCs and MoDCs cultured alone in complete media for 6 days. As a control, complete media were incubated for 6 days in the same conditions. All supernatants were filtered in 10 kDa columns before extraction. LC-HRMS metabolomics and lipidomics fingerprints were acquired on a Exactive Orbitrap mass spectrometer (Thermo Fisher Scientific) equipped with a Heated ElectroSpray Ionization (HESI) source operated in positive and negative electrospray ionization mode (ESI+ and ESI- respectively). Full instrument calibration was performed using ProteoMassT LTQ/FT-Hybrid ESI Pos/Neg (MERCK). Xcalibur software was used for the generation of all chromatographic peaks acquired in full scan mode. The chromatographic separation was performed with a high performance liquid chromatography (HPLC) system (1200 Infinity Series from Agilent Technologies).

For untargeted metabolomics, the analysis was done on a Hypersil Gold C_{18} column (2.1 mm × 100 mm i.d., 1.9 μm particle size, Thermo Fisher Scientific). Mobile phases consisted in water containing 0.1% acetic acid (A) and acetonitrile containing 0.1% acetic acid (B). The used elution gradient (A:B, v:v) was as follows: 95:5 from 0 to 2.40 min; 75:25 at 4.50 min; 30:70 at 11 min; 0:100 at 14 min to 16.5 min; 95:5 at 19 min to 25 min. The injected volume was 5 μL, the flow rate was 400 μL/min and the temperature of the column was maintained at 35°C.

For untargeted lipidomics analysis, the chromatographic separation was performed using a reverse phase CSH C_{18} (100 × 2.1 mm i.d., 1.7 μm particle size) column (Waters Corporation) using ACN:H_2O (60:40) and IPA:ACN:H_2O (88:10:2) as solvent A and B, respectively; both containing 10 mM ammonium acetate and 0.1% acetic acid. The programmed gradient was as follows (A:B, v:v): 60:40 at 0 min; 50:50 at 2 min; 30:70 at 12 min; 1:99 at 17 min; 60:40 at 26-30 min. The flow rate was maintained at 300 μL/min during the analysis. The column temperature was set at 45°C and the injection volume was 5 μL.

Results of mass spectrometry were compared with the data from Human Metabolome DataBase (HMDB). Heatmap was performed using Gene-E, using the metabolite relative quantity values. The relative quantity values are shown in z-score.

In Vivo Experiments

ATDC tracking was evaluated by the injection of gold labeled ATDCs. At the end of the differentiation of the ATDCs, 50-nm gold nanoparticles were added to each well. After one h of incubation at 37°C and 5% CO2, cells were harvested and washed 3 times in PBS. Cells were injected as described above in the experimental model section. Mice were sacrificed at day 3, day 6, day 10 and day 14. The presence of gold nanoparticles in different tissues was analyzed by Inductively Coupled Plasma Mass Spectrometry (ICP-MS) as previously described (Au mean of 3 biopsies/organ) (Managh et al., 2013, 2014). Briefly, the samples were digested in small volumes of concentrated acid. Following evaporation of the acid, a 5% aqua regia solution was used to reconstitute the samples. Analyses were performed on a sector-field ICP-MS instrument (Element 2XR; Thermo Scientific, Bremen, Germany). The instrument was fitted with a cyclonic spray chamber, a conical glass concentric nebulizer (both from Glass Expansion, West Melbourne, VIC, Australia), and a 0.25-mm inner diameter probe (Elemental Scientific, Omaha, NE). Gold is known to have a high affinity for the surfaces of the sample introduction system. Therefore, to minimize memory effects, solutions of 5% aqua regia and 10 mM cysteine were aspirated between samples.

To analyze ATDC phenotype *in vivo*, cells were labeled with Qtracker605 before injection according to the manufacturer instructions. Briefly, a 10nM labeling solution containing Qtracker Component A and Component B was prepared, incubated 5 min at room temperature and added to the cells (1x10^6 cells/mL) in complete medium. After 30 min incubation at 37°C and 5% CO2, cells were washed 3 times in PBS before injection. Animals were sacrificed 6 days later and spleen was collected and digested with collagenase D during 30 min at 37°C. ATDC staining was then performed on splenic cells and analyzed by flow cytometry.

To evaluate the engraftment of the human cells, blood cells were stained with anti-human CD45, anti-mouse CD45 and were then analyzed by flow cytometry. The engraftment of human cells was calculated as [% of human CD45$^+$ cells / (% of human CD45$^+$ cells + % of mouse CD45$^+$cells)]x100.

Lactate quantifications in blood at day 7 was measured by mass spectrometry (serum) or using ABL90 Flex Plus technology (blood gas, Radiometer, France).

To analyze *in vivo* mechanism of action of ATDCs, mice were sacrificed 21 days after injection of PBMC or PBMC/ATDCs. Blood cells were collected and splenocytes were prepared as described above before staining. CPD-labeled splenocytes (3 millions) were stimulated with 1μg/mL of plate-bound anti-CD3 (OKT3 clone) and 1μg/mL of soluble anti-CD28 (28.6 clone) in 24 well-plate for 3 days before measuring T cell proliferation by CPD dilution.

QUANTIFICATION AND STATISTICAL ANALYSIS

Statistical analysis was conducted using GraphPad Prism software. Results were expressed as the mean ± SEM and data were assumed to follow a normal distribution. As detailed in figure legends, group comparisons were made using 1way ANOVA, 2way ANOVA or Student's t tests (paired or unpaired). Survival curve was analyzed by log-rank (Mantel-Cox) test. *$p < 0.05$, **$p < 0.01$, *** $p < 0.001$. ''n'' corresponds to the number of individual donors or the number of individual mice analyzed.

DATA AND CODE AVAILABILITY

Microarray and Genomic Data Accession Numbers

We have deposited our microarray data in the Gene Expression Omnibus database (https://www.ncbi.nlm.nih.gov/geo). The accession numbers for the data reported in this paper are GEO: GSE104438.